Robust Beamforming for Collaborative MIMO-OFDM Wireless Systems

Byong-Ok Kwun

Department of Electrical & Computer Engineering
McGill University
Montreal, Canada

August 2007

A thesis submitted to McGill University in partial fulfillment of the requirements for the degree of Master of Engineering.

2007/08/22

Your file Votre référence
ISBN: 978-0-494-38485-5
Our file Notre référence
ISBN: 978-0-494-38485-5

Abstract

Collaborative beamforming is a powerful technique to increase communication energy efficiency and range in an energy-constrained network. To achieve high performance, collaborative beamforming requires accurate knowledge of channel state information (CSI) at the transmitters (collaborative nodes). In practice, however, such exact knowledge of CSI is not available. A robust transmitter design based on partial CSI is required to mitigate the effects of CSI mismatches.

This thesis focuses on the design and evaluation of a beamforming scheme that is robust to CSI mismatches for collaborative multiple-input multiple-output (MIMO) orthogonal frequency division multiplexing (OFDM) wireless systems. Using a max-min robust design approach, the robust beamformer is designed to maximize the minimum (worst-case) received signal-to-noise ratio (SNR) within a predefined uncertainty region at each OFDM subcarrier. In addition, several subcarrier power allocation strategies are investigated to further improve the robustness of collaborative systems. Numerical simulation results show that the robust beamformer offers improved performance over the nonrobust beamformers and the use of power allocation strategies among subcarriers further improves the system performance.

Sommaire

La formation de voie collaborative est une technique puissante afin d'augmenter l'efficacité et la plage d'énergie nécessaire à la communication dans un réseau ayant des contraintes énergétiques. Afin d'être performant, la formation de voie collaborative nécessite la connaissance exacte de l'information sur l'état du canal (CSI - *channel state information*) aux transmetteurs (noeuds collaboratifs). En pratique, cependant, cette information n'est pas disponible. La conception d'un transmetteur robuste fondé sur une CSI partielle est requise afin de pallier aux effets de l'inexactitude sur la CSI.

Cette thèse se concentre sur la conception et l'évaluation d'un algorithme de formation de voie collaborative robuste à l'inexactitude sur la CSI pour les systèmes sans fil à multiplexage par répartition orthogonale de la fréquence (OFDM - *orthogonal frequency division multiplexing*) à entrées multiples et sorties multiples (MIMO - *multiple-input multiple-output*). Utilisant une approche max-min robuste, le formateur de voie est conçu afin de maximiser le rapport signal sur bruit minimum reçu (le pire cas) à l'intérieur d'une région prédéterminée à chacune des sous-porteuses du OFDM. De plus, plusieurs stratégies d'allocation de puissance des sous-porteuses sont investiguées afin d'améliorer davantage la robustesse des systèmes collaboratifs. Les résultats de simulations numériques montrent que le formateur de voie robuste offre de meilleures performances que les formateurs de voie non robustes et que l'utilisation des stratégies d'allocation de puissance des sous-porteuses améliore encore davantage les performances du système.

Acknowledgments

I would like to thank my supervisor, Prof. Benoît Champagne, for his guidance and support throughout my graduate studies. I am very grateful to Prof. Champagne for his financial support to carry out my research. I would also like to thank Dr. Amr El-Keyi for providing vector channel simulator MATLAB programs that were used in my research. Moreover, I would like to thank Dr. El-Keyi for his great technical support during my research.

I am grateful to all my friends and colleagues in the Telecommunications and Signal Processing Laboratory, past and present. I would like to express my thanks to Patrick Kechichian, Wei Chu, Eric Plourde, Benoît Pelletier, François Duplessis-Beaulieu, and Bo Gao. I am especially thankful to Eric Plourde for the French translation of the thesis abstract.

I would particularly like to thank my beautiful wife, Ji-Suk Kwak, for her love, support, and understanding during the course of this work. I would also like to thank my parents, my sister, my brother-in-law, and my niece for their unconditional love and support throughout my studies at McGill University. Finally, I dedicate this thesis to the loving memory of my late grandfather, Bong-Su Kwun, and my late grandmother, Myong-Suk Oh.

Contents

List of Figures

List of Tables

Notation

$\mathbf{X}^T$	Transpose of matrix $\mathbf{X}$
$\mathbf{X}^*$	Conjugate of matrix $\mathbf{X}$
$\mathbf{X}^H$	Conjugate transpose (Hermitian) of matrix $\mathbf{X}$
$E\{\mathbf{X}\}$	Expectation of matrix $\mathbf{X}$
$tr\{\mathbf{X}\}$	Trace of matrix $\mathbf{X}$
$\|x\|$	Absolute value of scalar x
$\|\mathbf{x}\|$	Euclidean norm of vector $\mathbf{x}$: $\|\mathbf{x}\| = \sqrt{\mathbf{x}^H\mathbf{x}}$
$\|\mathbf{X}\|_F$	Frobenius norm of matrix $\mathbf{X}$: $\|\mathbf{X}\|_F = \sqrt{\mathrm{tr}\{\mathbf{X}^H\mathbf{X}\}}$
$\mathrm{diag}\{\mathbf{x}\}$	Diagonal matrix with entries of $\mathbf{x}$ on its main diagonal
$\mathbf{I}_P$	$P \times P$ identity matrix
$\triangleq$	Defined as
$\ln(\cdot)$	Natural logarithm
$*$	Convolution operator
$(\cdot)_N$	Modulo N
$J_n(\cdot)$	nth order Bessel function of the first kind
δ_{jl}	Kronecker delta: $\delta_{jl} = \begin{cases} 1 & j = l \\ 0 & j \neq l \end{cases}$
$(x)^+$	$\max(0, x)$

List of Acronyms

16-QAM	16-Quadrature Amplitude Modulation
AWGN	Additive White Gaussian Noise
BEP	Bit Error Probability
BER	Bit Error Rate
BS	Base Station
BPSK	Binary Phase Shift Keying
CSI	Channel State Information
CP	Cyclic Prefix
DFT	Discrete Fourier Transform
EVD	Eigenvalue Decomposition
FFT	Fast Fourier Transform
ICI	Inter Carrier Interference
IDFT	Inverse Discrete Fourier Transform
IFFT	Inverse Fast Fourier Transform
i.i.d.	Independent and Identically Distributed
ISI	Inter Symbol Interference
KKT	Karush-Kuhn-Tucker
MIMO	Multiple-Input Multiple-Output
MMSE	Minimum Mean Square Error
MRC	Maximum Ratio Combiner
OECG	Overall Effective Channel Gain
OFDM	Orthogonal Frequency Division Multiplexing
pdf	Probability Density Function
SDMA	Space-Division Multiple Access

SEP	Symbol Error Probability
SER	Symbol Error Rate
SNR	Signal-to-Noise Ratio
STBC	Space-Time Block Code
QAM	Quadrature Amplitude Modulation
QPSK	Quadrature Phase Shift Keying
WCN	Wireless Cellular Network
WLAN	Wireless Local Area Network
WSN	Wireless Sensor Network
ZMCSCG	Zero Mean Circularly Symmetric Complex Gaussian

Chapter 1

Introduction

Rapid advancement of electronics has permitted enormous growth in wireless communications. Moreover, this technological advance has allowed the design of low-cost, low-power, and small-sized network devices that can be used in a wide range of wireless applications. A system of distributed microsensors, for example, can monitor an area and detect, identify, localize, and track an object for environmental monitoring, military operations, industrial automation, and traffic control [1, 2].

Distributed nodes in wireless networks are required to transmit to or receive from a remote location. Most often, the communication range is limited by the transmission power level of the individual network nodes since each node is usually operated by a limited power source such as a battery. In this energy-constrained network, cooperative communication techniques can greatly increase the energy efficiency and range of communication [3]. One technique of cooperative communication that has recently received great attention is *collaborative or distributed beamforming* [4–13]. In the transmit version of this technique, a cluster of nodes shares the same data *a priori* and cooperatively forms a beam in the direction of interest with a high power concentration as illustrated in Fig. 1.1. Collaborative beamforming using a random array can theoretically produce up to an M-fold gain in the received signal-to-noise ratio (SNR) for a network of M distributed nodes similar to conventional beamforming using a uniform linear array. In addition to the high directional transmit gain (directivity), a cluster of nodes can receive data from the direction of interest while attenuating interference from other directions. These properties of collaborative beamforming enable space-division multiple access (SDMA) scheme among clusters [4–6].

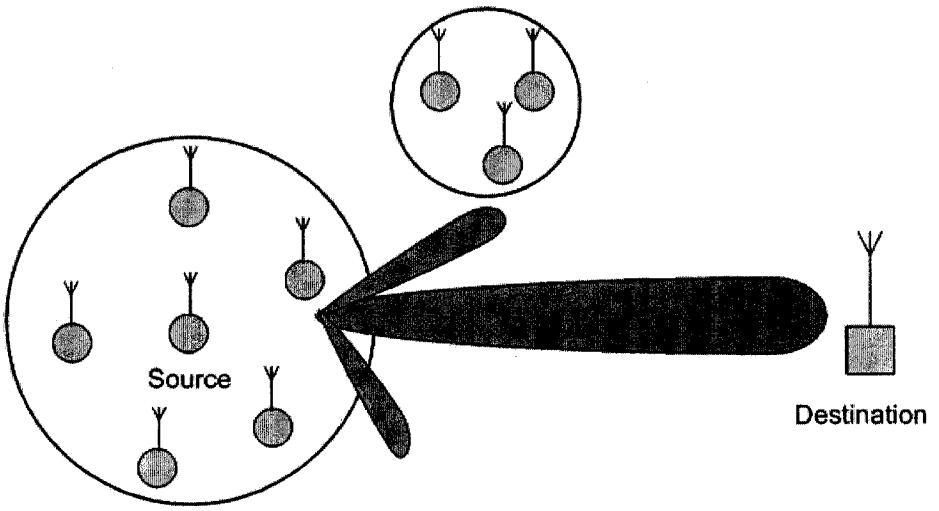

Fig. 1.1 Collaborative beamforming concept in wireless networks.

Hence, collaborative beamforming can increase communication range without increasing the power of individual nodes or save transmission power for a given communication channel.

The rest of this chapter provides a brief literature review on collaborative beamforming and the motivation, contribution, and organization of the thesis.

1.1 Literature Review

Recently, collaborative beamforming has become an extensive research topic in wireless communications due to its great potential to increase communication efficiency. Previous studies have mainly focused on the application of wireless sensor network (WSN). However, theses studies can be easily extended to support other wireless communications applications such as wireless cellular network (WCN) and wireless local area network (WLAN).

Authors in [4–6] study theoretical beampatterns of collaborative beamforming for distributed wireless *ad hoc* sensor networks in a probabilistic sense. Using ideal channel and system models, the authors show that an average beampattern with a narrow mainlobe, low sidelobes, and a high directional gain can be realizable by using a sufficient number of randomly distributed nodes. In addition, the study includes the exact and Gaussian-approximated distribution of the beampatterns and sidelobes as well as the effects of initial

phase and location estimation errors on the average beampattern. However, practical issues such as the effects of time-varying multipath fading channels and synchronization error on the average spatial directivity patterns are not investigated.

A major obstacle to implementing collaborative beamforming is that the location of nodes is *a priori* unknown. Nodes in the same cluster must have an ability to dynamically coordinate and synchronize with each other. In [7–9], the authors propose a carrier phase synchronization protocol for clustered wireless sensor networks using a *master-slave* architecture. The proposed transmit beamforming process can be summarized as follows. One of the nodes in the cluster is selected as a master node. The designated master node which acts as a reference node broadcasts a carrier synchronization signal to the slave nodes. Each slave node then compensates for the delay of the synchronization signal, resulting in phase and frequency synchronization. When the destination (receiver) node sends out a beacon signal, the source nodes adjust their initial phase based on the beacon and then coherently transmit a common message signal to the destination. The effects of the phase synchronization errors on beamforming gains are also analyzed using a flat Rayleigh fading transmission model. Importantly, it is shown that a high beamforming gain can still be achieved using collaborative beamforming in the presence of synchronization errors.

Based on the study in [7–9], an alternative distributed beamforming approach employing a simple feedback control has been investigated in [10–12]. Each collaborating node in the cluster first modulates a common message signal with a random phase offset rather than with an estimated phase offset obtained from a beacon signal as proposed in [7–9]. Then, the destination node measures SNR and sends back a one-bit feedback signal, which indicates the current signal strength, to the source nodes. If the SNR is better than the previous one, each node keeps the current phase value, otherwise, each node reverts to the previous one. Then, each node introduces another random perturbation to its phase and repeats the process. In addition, the authors show that this random phase process asymptotically converges to a perfect phase coherent system.

Lastly, the authors in [13] study feasible energy savings from collaborative beamforming for a remote low power wireless sensor network. The study includes the relationship between overall energy savings and network sizes.

1.2 Thesis Motivation and Contribution

Although the recent studies on collaborative beamforming have shown very promising results, the analysis is based on simple channel and system models. Moreover, accurate knowledge of channel state information (CSI) is assumed to be available at the transmitters (collaborative nodes), typically through channel feedback. In a practical situation, however, the transmitters cannot have exact knowledge of instantaneous CSI due to the time-varying characteristics of channels, channel estimation error, and delay in channel feedback. In such a situation, a robust design is required to mitigate the effects of CSI uncertainties. There are two different robust design approaches. In the Bayesian approach, the statistics of the error are utilized to design robust beamformers (*e.g.*, [14, 15]). In the max-min approach, robust beamformers are designed based on the worst-case performance optimization (*e.g.*, [16–18]).

Orthogonal frequency division multiplexing (OFDM) has recently become very popular in high data rate wireless communications due to its robustness against frequency selective fading, simple channel equalization, and easy modulation/demodulation. These properties of OFDM motivate its use as a basic modulation technique in the study of collaborative beamforming. In an OFDM based collaborative transmission model, a network of nodes can cooperatively form a *virtual antenna array* to transmit common messages to a remote receiver using multicarriers.

In this thesis, we focus on the design and evaluation of a beamforming scheme that is robust against CSI mismatches and applicable to practical collaborative wireless systems. Our aim is to extend the max-min robust beamforming design approach of [17] into a multiple-input multiple-output (MIMO) OFDM framework for collaborative transmission systems. The robust beamformer is designed to provide the best performance in worst-case scenario by maximizing the minimum received SNR within a predefined uncertainty set associated with the current CSI estimate. We show that the robust design takes full advantage of the available estimated eigenmodes of the channel while the nonrobust design uses only the maximum one. Specifically, at each OFDM subcarrier, the robust beamformer forms beams along the eigenvectors of the presumed transmit channel correlation matrix with a water-filling type of power loading across the channel eigenmodes.

The performance of OFDM systems can be substantially degraded by subcarriers experiencing deep fades. In other words, the overall bit error rate (BER) performance is

mainly dominated by attenuated subcarriers. Appropriate distribution of transmission power among subcarriers can minimize the performance degradation. In this thesis, we also extend the power allocation strategies considered in [19, 20] for the nonrobust design approach to the case of robust beamforming. The optimization criteria include the maximization of the arithmetic, geometric, harmonic, and minimum means of SNRs.

Through simulations, the performance of the proposed robust beamformer is compared with the conventional one-directional (1-D) beamformer and the equal-power beamformer using uncoded symbol error rate (SER) performance results from Monte-Carlo simulations. Transmission channels between the collaborative nodes and the receiver are modeled as wideband multi-path vector channels [21]. Simulations are conducted under two CSI mismatch scenarios: downlink measurements and delayed channel feedback. Each scenario defines how to obtain partial CSI. Numerical simulation results show that the robust beamformer offers improved performance over the conventional one-directional and equal-power beamformers. Incorporating subcarrier power allocation strategies into the simulations, it is shown that subcarrier power allocation further improves the system performance.

1.3 Thesis Organization

The rest of the thesis is organized as follows. Chapter 2 provides an overview of collaborative beamforming and basic principles of OFDM. In Chapter 3, we provide a system model for MIMO-OFDM wireless communication systems using collaborative transmission, including system block diagrams. In addition, a robust beamforming scheme for collaborative MIMO-MIMO wireless systems is derived based on worst-case performance optimization. Chapter 4 describes power allocation strategies to distribute the total available power at the transmitters to OFDM subcarriers. Numerical simulation results and discussion are presented in Chapter 5. Chapter 6 concludes the thesis with a brief summary and future research directions.

Chapter 2

Background

This chapter provides the necessary background knowledge for understanding the material presented in this thesis. A brief overview of collaborative beamforming, including the beampattern, directivity, and beamforming gain of random arrays is presented in Section 2.1. The basic principles of OFDM are discussed in Section 2.2.

2.1 Overview of Collaborative Beamforming

Collaborative beamforming is an efficient way to form a high directional beam toward a desired target direction in a distributed wireless system. A simple protocol for collaborative beamforming depicted in Fig. 2.1 can be described as follows. The destination node periodically sends out a beacon to the source nodes. Each node then adjusts its initial phase to the phase of the beacon. Assuming perfect carrier frequency and time synchronization within a cluster of nodes and a common message to be transmitted is available for all nodes, the source nodes steer a beam to the destination node with high directivity. It is, therefore, of particular interest to investigate beampatterns and directivity of random arrays [4,6] and a maximum achievable beamforming gain using collaborative beamforming [7–9]. The main results of these studies are presented in the following subsections.

2.1.1 Average Beampattern

Consider M nodes randomly and uniformly placed over a disk of radius R with the position of the kth node denoted by (r_k, θ_k) as shown in Fig. 2.1. The array factor that is the array

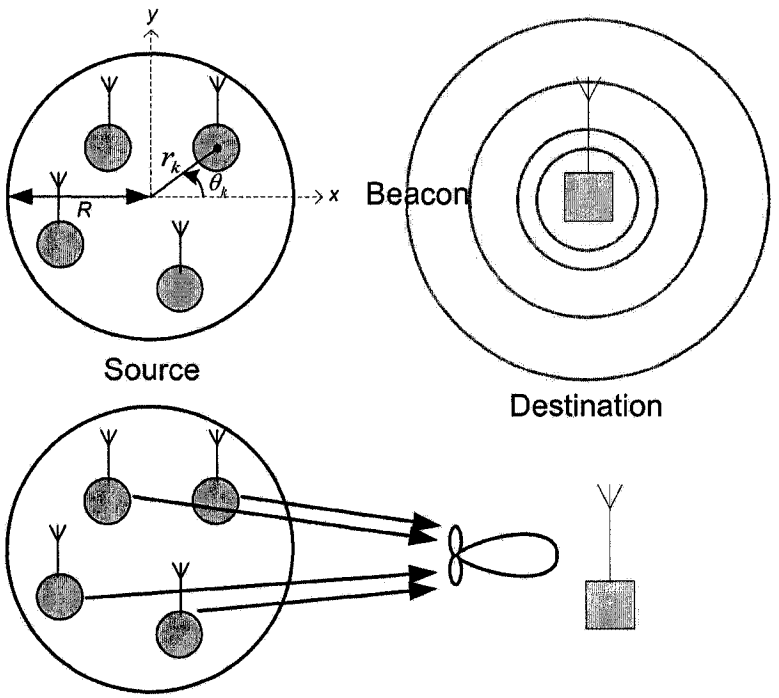

Fig. 2.1 A simple protocol for collaborative beamforming.

response to a plane wave in a given signal propagation direction for a given location of nodes $\mathbf{r} = [r_1, r_2, \ldots, r_M]$ and $\boldsymbol{\theta} = [\theta_1, \theta_2, \ldots, \theta_M]$ can be expressed as

$$F(\phi|\mathbf{r}, \boldsymbol{\theta}) = \frac{1}{M} \sum_{k=1}^{M} e^{j\frac{2\pi}{\lambda} r_k [\cos(\phi_0 - \theta_k) - \cos(\phi - \theta_k)]} \tag{2.1}$$

where λ is the wavelength of the carrier frequency, ϕ_0 is the look direction, and ϕ is the scanning angle [22]. Assuming $\phi_0 = 0$, the array factor (2.1) can be written as

$$F(\phi|\mathbf{z}) = \frac{1}{M} \sum_{k=1}^{M} e^{-j4\pi \frac{R}{\lambda} \sin(\frac{\phi}{2}) z_k} \tag{2.2}$$

where $\mathbf{z} = [z_1, z_2, \ldots, z_M]$ and $z_k = \frac{r_k}{R} \sin(\theta_k - \frac{\phi}{2})$ is a compound random variable associated to the kth node. The probability density function (pdf) of z_k is

$$f_{z_k}(z) = \frac{2}{\pi} \sqrt{1 - z^2}, \quad -1 \leq z \leq 1. \tag{2.3}$$

Then, the beampattern or radiation pattern can be obtained as the squared magnitude of the array factor:

$$\begin{aligned} P(\phi|\mathbf{z}) &\triangleq |F(\phi|\mathbf{z})|^2 \\ &= \frac{1}{M} + \frac{1}{M^2}\sum_{k=1}^{M} e^{-j\alpha(\phi)z_k} \sum_{\substack{l=1 \\ l\neq k}}^{M} e^{j\alpha(\phi)z_l} \end{aligned} \tag{2.4}$$

where $\alpha(\phi) = 4\pi\frac{R}{\lambda}\sin\frac{\phi}{2}$. Averaging over all realizations of $\mathbf{z}$, the average beampattern is obtained as

$$\begin{aligned} P_{av}(\phi) &\triangleq E_{\mathbf{z}}\{P(\phi|\mathbf{z})\} \\ &= E_{\mathbf{z}}\left\{\frac{1}{M} + \frac{1}{M^2}\sum_{k=1}^{M}(\cos(\alpha(\phi)z_k) - j\sin(\alpha(\phi)z_k))\right. \\ &\quad \left.\cdot \sum_{l=1,l\neq k}^{M}(\cos(\alpha(\phi)z_l) + j\sin(\alpha(\phi)z_l))\right\} \\ &= \frac{1}{M} + \frac{1}{M^2}(M^2 - M)E_{\mathbf{z}}\{\cos(\alpha(\phi)z_k)\cos(\alpha(\phi)z_l)\} \\ &= \frac{1}{M} + \left(1 - \frac{1}{M}\right)\left|2\frac{J_1(\alpha(\phi))}{\alpha(\phi)}\right|^2. \end{aligned} \tag{2.5}$$

The corresponding average beampattern is plotted in Fig. 2.2 for several values of M and R. As can be seen, the mainlobe width of the average beampattern becomes narrower as the radius R becomes lager whereas the average power level of the sidelobe becomes smaller as the number of the collaborative nodes increases. In addition, it can be observed that the average power level of the sidelobe approaches to $1/M$, which corresponds to the first term in (2.5), as the observation angle moves away from the broadside.

Fig. 2.3 shows one particular realization of randomly generated node locations and the corresponding beampattern. The average beampattern is also plotted in the figure to compare with the realization. The mainlobe of the average beampattern is very closely matched to the realization. However, the sidelobes of the realization are different from those of the average beampattern.

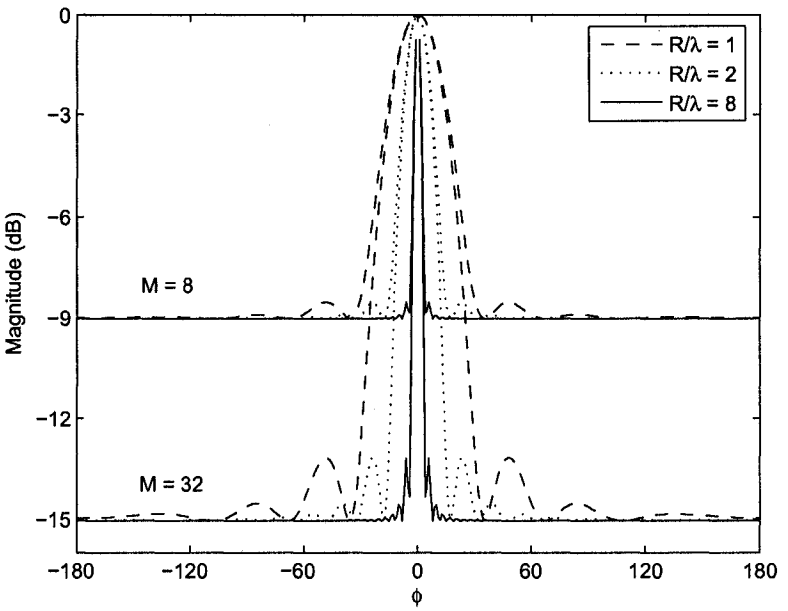

Fig. 2.2 Average beampattern for different values of M and R.

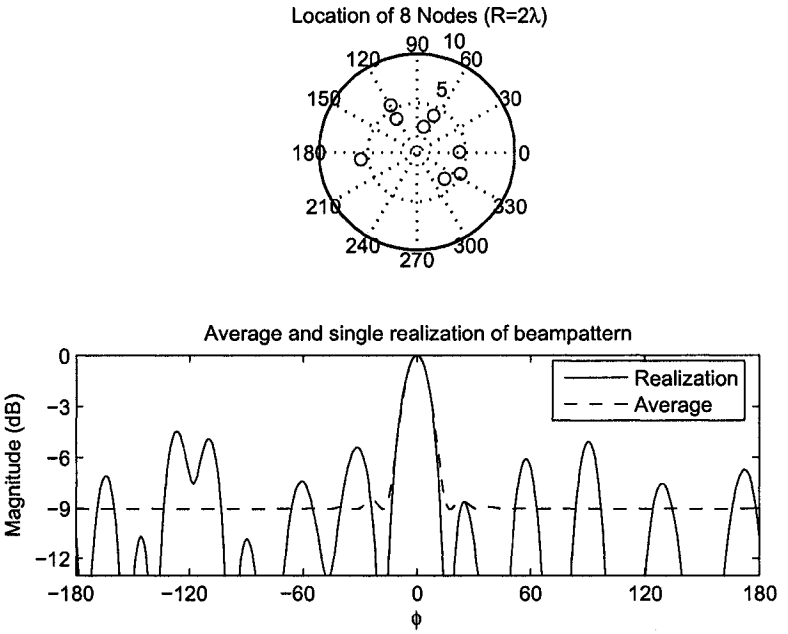

Fig. 2.3 Average and single realization of beampattern with $R/\lambda = 2$ and $M = 8$.

2.1.2 Average Directivity

Directivity measures how much the radiation pattern is concentrated in the direction of interest. It is defined as the ratio of the radiated energy in the look direction ($\phi_0 = 0$) to the total radiated power:

$$D(\mathbf{z}) \triangleq \frac{2\pi P(0|\mathbf{z})}{\int_{-\pi}^{\pi} P(\phi|\mathbf{z})d\phi}. \tag{2.6}$$

Averaging over all realizations of $\mathbf{z}$ and using Jensen's inequality, $\varphi(E\{X\}) \leq E\{\varphi(X)\}$ for a convex function φ, the lower bound of the average directivity is given by

$$D_{av} \triangleq E_{\mathbf{z}}\{D(\mathbf{z})\} \geq \frac{M}{1 + 0.09332\lambda\frac{M}{R}}. \tag{2.7}$$

The proof is given in [6]. Fig. 2.4. shows the average normalized directivity D_{av}/M obtained from numerical simulations and the corresponding lower bounds for different values of M. Note that the simulation results are obtained by averaging 1000 realizations. It can be observed that the lower bounds are very close to the simulation results and the average normalized directivity increases as the radius R increases. Thus, for a given number of nodes, a higher directivity can be achieved by having nodes placed in a larger disk.

2.1.3 Beamforming Gain

Considering a cluster of M nodes that transmit a common message signal $m(t)$ to a remote destination such as a Base Station (BS), a basic communication model is illustrated in Fig. 2.5. The baseband representation of the received signal with the total transmission power $P_0 = 1$ can be expressed as [1]

$$r(t) = \sum_{i=1}^{M} \frac{1}{\sqrt{M}} w_i^* h_i e^{j\phi_i} m(t) + n(t) \tag{2.8}$$

where i is the node index, w_i is the beamforming weight, h_i is the channel attenuation factor, which is modeled as a zero mean circularly symmetric complex Gaussian (ZMCSCG) random variable with unit variance, ϕ_i is the phase synchronization error, and $n(t)$ is the additive white Gaussian noise (AWGN). Using spatial matching ($w_i = h_i$), the beamforming

[1] Under the narrowband assumption, we can assume that the message signals arrived at the destination node synchronously, *i.e.*, $m(t) \approx m(t - \tau_i)$ where τ_i represents the different propagation.

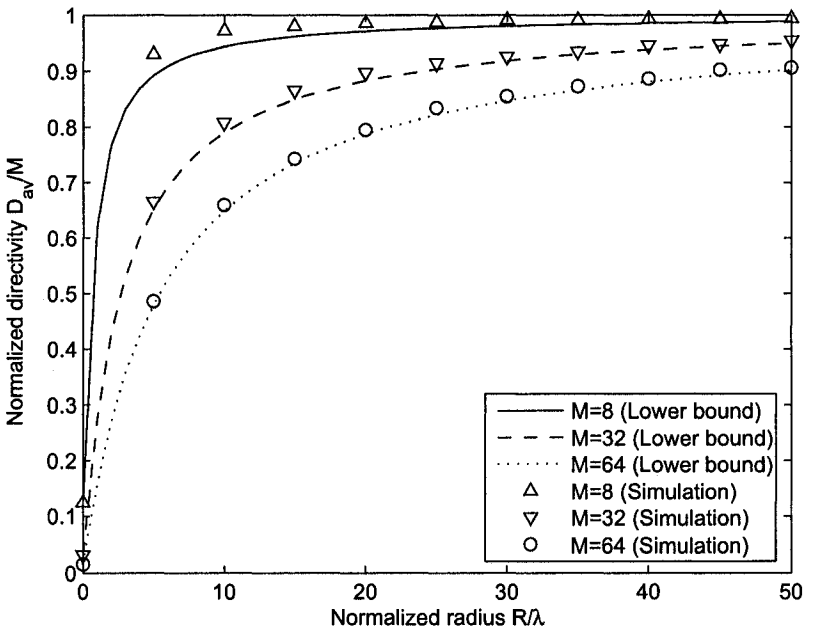

Fig. 2.4 Normalized directivity D_{av}/M.

gain or received signal power is given by

$$P_R = M \left\| \frac{1}{M} \sum_{i=1}^{M} |h_i|^2 e^{j\phi_i} \right\|^2 . \tag{2.9}$$

Motivated by the law of large numbers [23], we may argue that

$$\frac{1}{M} \sum_{i=1}^{M} |h_i|^2 e^{j\phi_i} \rightarrow E\{|h_i|^2 e^{j\phi_i}\} \ a.s. \tag{2.10}$$

as M increases, where *a.s.* denotes almost sure convergence. Modeling $|h_i|^2$ $(i = 1, \ldots, M)$ as independent and identically distributed (i.i.d.) exponential random variables with unit mean, which are independent from the phase errors ϕ_i, (2.10) is reduced to $E\{\cos(\phi_i)\}$. Hence, it is found that the normalized beamforming gain $\frac{1}{M}P_R$ converges to $(E\{\cos(\phi_i)\})^2$ as $M \rightarrow \infty$. Note that in case of no phase error, $\frac{1}{M}P_R$ converges to 1. For finite M, it can

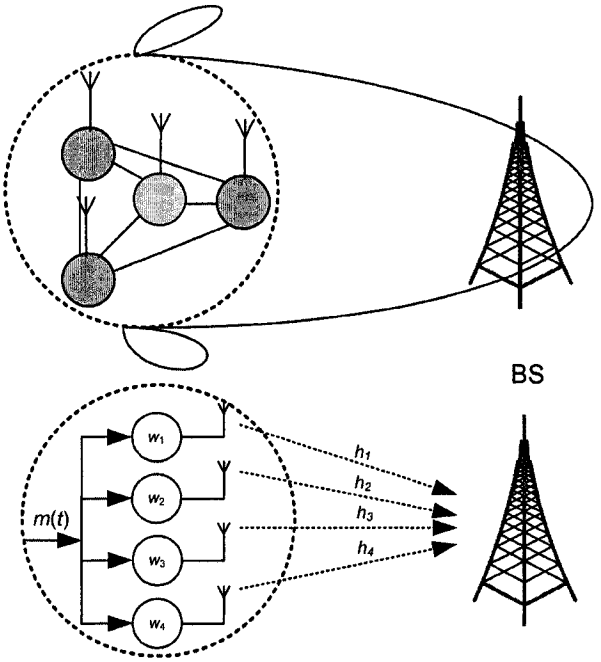

Fig. 2.5 A virtual antenna array for collaborative beamforming.

be readily shown that

$$E\{P_R\} = 1 + (M-1)E\{\cos(\phi_i)\}^2. \tag{2.11}$$

When there is no phase error, $E\{P_R\}$ reduces to M, which reflects the M-fold beamforming gain.

Assuming that the phase synchronization error ϕ_i is uniformly distributed between $-\pi\Delta$ and $\pi\Delta$, where Δ is the phase error parameter, the analytical and simulation results of the normalized expected value of the beamforming gain (2.11) against several different values of the phase error parameter Δ are plotted in Fig. 2.6. In addition, Fig. 2.7 shows the expected value of the beamforming gain with the number of nodes M. As can be observed, collaborative beamforming with imperfect synchronization ($\Delta = 0.4$) provides more than 65% of the maximum achievable beamforming gain. Fig. 2.8 depicts the effect of phase error on the BER performance. Note that binary phase shift keying (BPSK) is used for the BER simulation. It is found that the phase error causes approximately 1dB loss in case of $M = 4$. Therefore, collaborative beamforming can still provide a significant performance gain in the presence of synchronization errors as compared with a single antenna transmission.

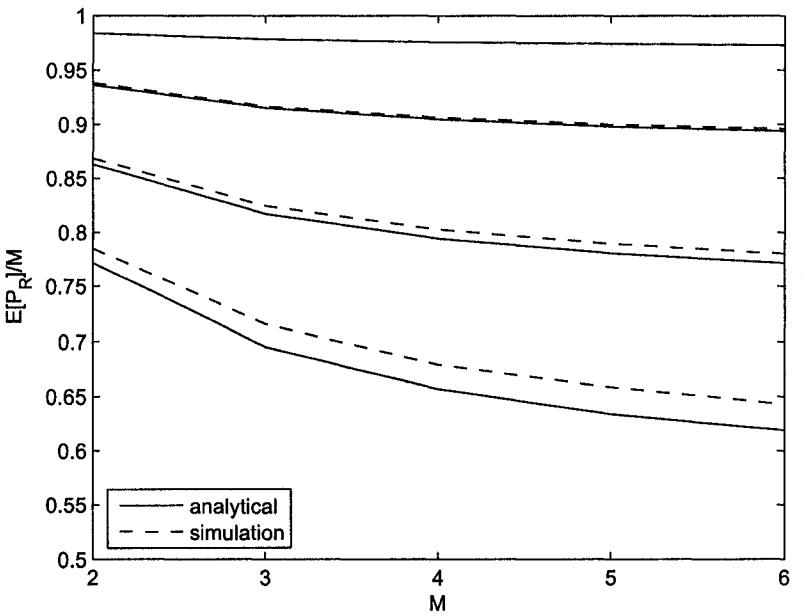

Fig. 2.6 $E\{P_R\}/M$ vs. M for $\Delta = 0.1$, 0.2, 0.3, and 0.4 (top to bottom).

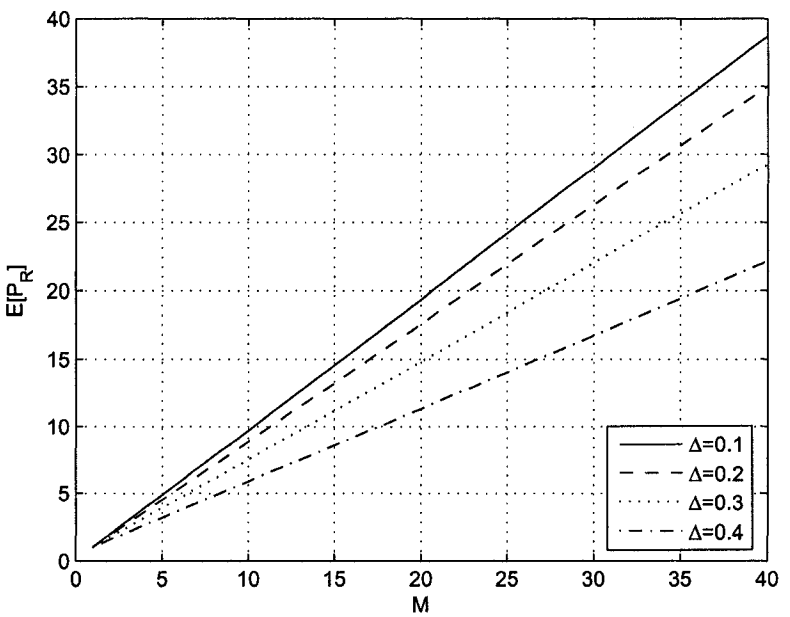

Fig. 2.7 $E\{P_R\}$ vs. M for $\Delta = 0.1$, 0.2, 0.3, and 0.4.

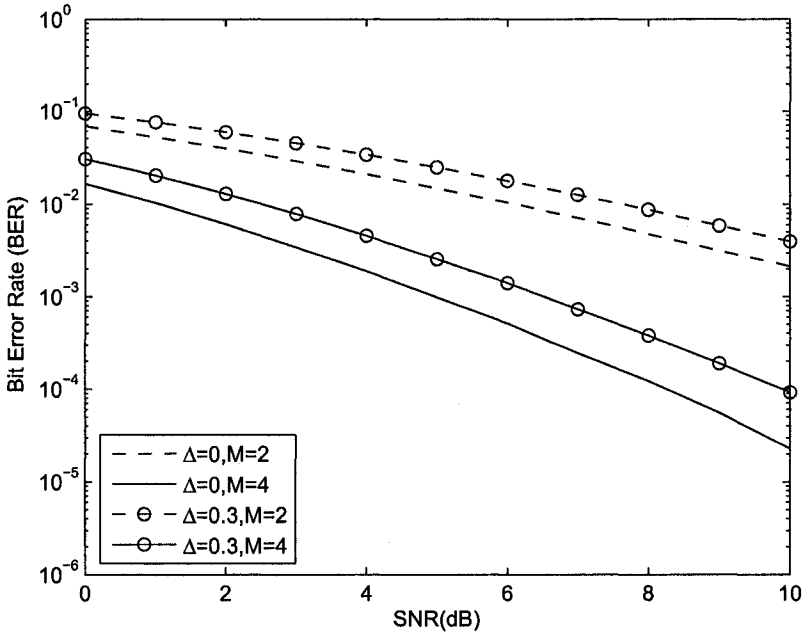

Fig. 2.8 BER vs. SNR for $\Delta = 0$ and 0.3.

2.2 Basic Principles of Orthogonal Frequency Division Multiplexing

OFDM is a multicarrier modulation technique that equally divides the available frequency spectrum into different subchannels and distributes the transmitted bitstream over these subchannels [24, 25]. In other words, OFDM transforms a high-rate bitstream into several low-rate bitstreams that are transmitted over subchannels whose bandwidth is narrower than the coherence bandwidth of the full channel. This can be ensured by choosing an appropriate number of subchannels and maintaining orthogonality between them. In this multicarrier system, a broadband multipath fading channel is effectively converted into a number of parallel narrowband flat fading channels, so channel equalization is simplified.

Despite these benefits, OFDM was not widely used in wireless communications due to the high implementation complexity of modulation. However, recent advances in digital signal processing technologies have enabled widespread use of OFDM in wireless communications by offering simple and cheap implementations of the discrete Fourier trans-

form (DFT) and inverse DFT (IDFT) [24, 25]. In this digital implementation, OFDM symbols are generated and recovered using inverse fast Fourier transform/fast Fourier transform (IFFT/FFT), which are computationally efficient algorithms for computing the IDFT/DFT. Moreover, by inserting a cyclic prefix (CP) in front of each OFDM symbol, inter symbol interference (ISI) and inter carrier interference (ICI) can be eliminated.

In the following subsections, after discussing the orthogonality principle, we present basic baseband OFDM transceivers and the CP.

2.2.1 Orthogonality

Two functions of the real variable t, $u_1(t)$ and $u_2(t)$, are said to be orthogonal to each other if their inner product is zero:

$$\int_a^b u_1(t)u_2^*(t)dt = 0. \tag{2.12}$$

Consider an OFDM system in which the available frequency bandwidth is divided into N frequency bins. The equally spaced carrier frequencies can be expressed as

$$f_k = k\frac{B}{N} \tag{2.13}$$

where B is the total available bandwidth and $k = 0, 1, \ldots, N-1$. Now consider the complex exponential carrier signals

$$\psi_k(t) = e^{j2\pi f_k t}, \quad k \in \{0, 1, \ldots, N-1\}. \tag{2.14}$$

We can then see that a set of carrier signals satisfy the orthogonal relationship in (2.12):

$$\frac{1}{T_s}\int_0^{T_s} \psi_k(t)\psi_n^*(t)dt = \begin{cases} 0, & k \neq n \\ 1, & k = n \end{cases} \tag{2.15}$$

where $T_s = N/B$ is the OFDM symbol time. Equation (2.15) implies that each carrier frequency chosen as an integer multiple of the inverse of the OFDM symbol time ensures orthogonality between subchannels in OFDM systems. Fig. 2.9 illustrates the orthogonality of carriers in the frequency domain. Each sinc function represents a specific carrier due to the rectangular pulse shaping in the time domain. In addition, overlapping carriers improves spectral efficiency of multicarrier modulation without creating interference since

each carrier is in the nulls of all of the other carriers. Therefore, maintaining orthogonality of carriers without compromising system bandwith is a key factor to transmit multiple bitstreams over parallel channels without distortion.

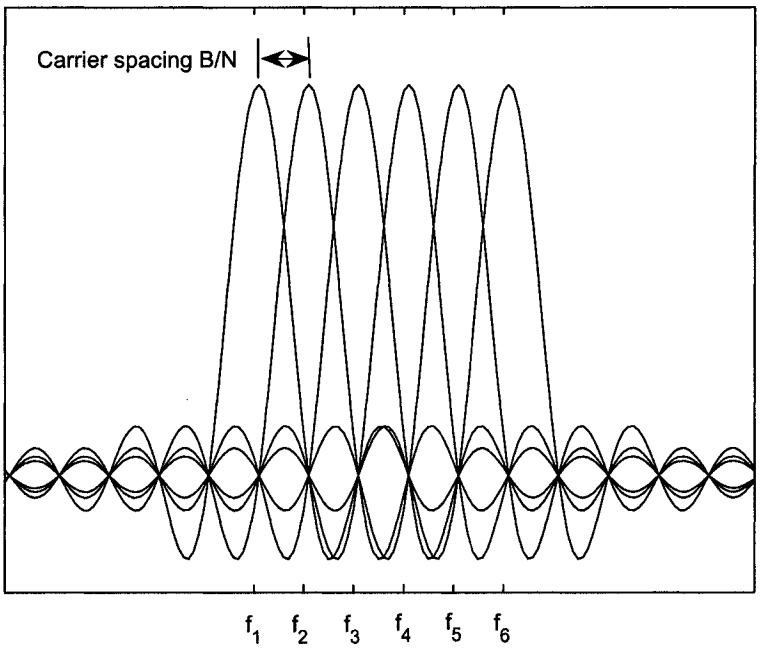

Fig. 2.9 Frequency response of OFDM subcarriers.

2.2.2 Basic Baseband OFDM Transceivers

Consider an OFDM system with N subcarriers. The block diagram of an OFDM baseband model with a single transmit antenna and a single receive antenna is depicted in Fig. 2.10. At the transmitter, the input datastream is first mapped according to the quadrature amplitude modulation (QAM) modulator, resulting in a series of complex symbols (IQ symbols) at the rate B. The corresponding sequence of complex symbols (each having a duration $T = 1/B$) is then converted into N parallel complex symbol substreams (OFDM symbol duration $T_s = NT$) by the serial-to-parallel (S/P) converter. The resulting block of N symbols is denoted by the vector $\mathbf{s} = [s(0), s(1), \ldots, s(N-1)]^T$. Using the IDFT, the N complex frequency components are transformed into the time domain sequence

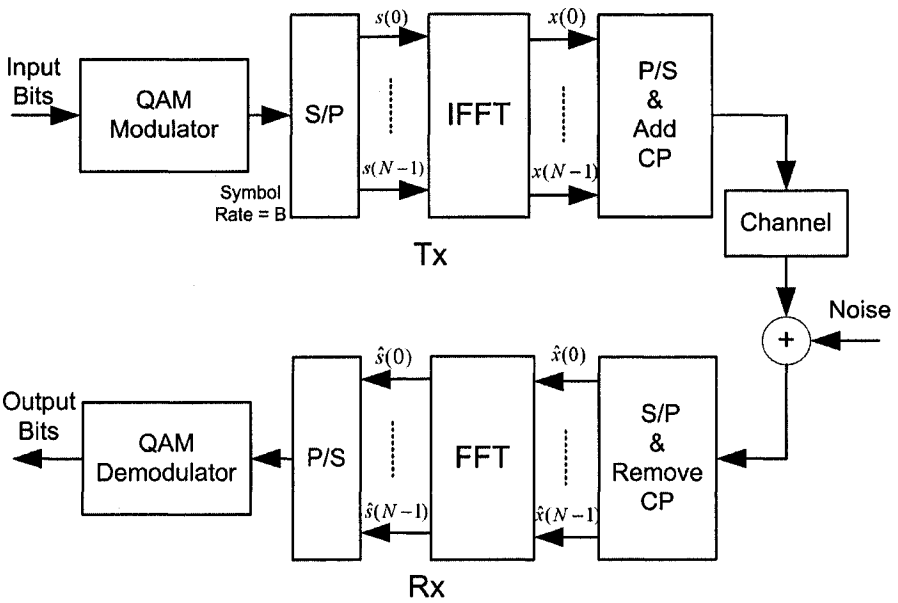

Fig. 2.10 Block diagram of a baseband OFDM system.

$\mathbf{x} = [x(0), x(1), \ldots, x(N-1)]^T$ whose elements are given by

$$x(n) = \frac{1}{\sqrt{N}} \sum_{k=0}^{N-1} s(k) e^{\frac{j2\pi nk}{N}}, \quad 0 \leq n \leq N-1. \tag{2.16}$$

Note that the corresponding time domain samples are equivalent to sampling the analog multicarrier signal generated by N orthogonal subcarrier frequencies at instances $t = nT_s/N$:

$$x(t) = \frac{1}{\sqrt{N}} \sum_{k=0}^{N-1} s(k) e^{j2\pi f_k t}. \tag{2.17}$$

The N time domain samples are then transmitted to the receiver after the parallel-to-serial (P/S) conversion.

Assuming an AWGN channel between the OFDM transmitter and receiver, the time domain samples corrupted by additive noise can be expressed as

$$\hat{x}(n) = x(n) + \eta(n), \quad 0 \leq n \leq N-1 \tag{2.18}$$

where $\eta(n)$ is an additive noise term. After the S/P converter, a set of N parallel received samples can be represented by a vector $\hat{\mathbf{x}} = [\hat{x}(0), \hat{x}(1), \ldots, \hat{x}(N-1)]^T$. The time samples are then converted back into frequency samples by the DFT operation:

$$\hat{s}(k) = \frac{1}{\sqrt{N}} \sum_{n=0}^{N-1} \hat{x}(n) e^{-\frac{j2\pi nk}{N}}, \quad 0 \leq k \leq N-1 \tag{2.19}$$

where $\hat{s}(k)$ is the estimate of the complex symbol for subcarrier k. Once the QAM parallel symbols are converted into serial format, the received bitstream can be recovered by the QAM demodulator. In practice, the number of subcarriers N is selected to be a power of two to increase computational efficiency of the IDFT/DFT operations via the IFFT/FFT.

2.2.3 The Cyclic Prefix

An OFDM system divides the available frequency spectrum into different orthogonal subchannels and transforms a high-rate datastream into a number of low-rate substreams. By choosing a proper number of subchannels, we can ensure that the bandwidth of the subchannel is less than that of the original channel. Hence, multicarrier modulation can effectively mitigate the effect of the frequency-selective fading channel. However, a delay-dispersive channel still can cause loss in orthogonality among subcarriers, leading to ICI, and cause ISI between successive OFDM symbols in case of a series of OFDM symbols being transmitted. Fortunately, by inserting a cyclic redundancy to OFDM symbols, known as a guard interval or a CP, both ISI and ICI can be eliminated completely.

Consider an OFDM symbol $\mathbf{x} = [x(0), x(1), \ldots, x(N-1)]^T$ of length N in (2.16) and a frequency-selective channel with the baseband sampled channel impulse response (sampling interval $T = 1/B$) $\mathbf{g} = [g(0), g(1), \ldots, g(L-1)]^T$ of length L. Then, we can construct a new sequence by appending the last $L-1$ samples of $\mathbf{x}$, $x(N-L+1), \ldots, x(N-1)$, to the front of each sequence of OFDM symbols. The new sequence becomes $\tilde{\mathbf{x}} = [\tilde{x}(-L+1), \ldots, \tilde{x}(N-1)]^T = [x(N-L+1), \ldots, x(N-1), x(0), \ldots, x(N-1)]^T$ of length $N+L-1$ as shown in Fig. 2.11. Note that the duration of the new OFDM symbol is $T_s = (N+L-1)/B$. After the CP insertion, the new sequence $\tilde{\mathbf{x}}$ is transmitted serially through a channel. Then, the received signal can be expressed as a linear convolution of the transmitted signal $\tilde{x}(n)$ for $0 \leq n \leq N-1$ and the sampled channel impulse response $g(n)$ for $0 \leq n \leq L-1$, plus

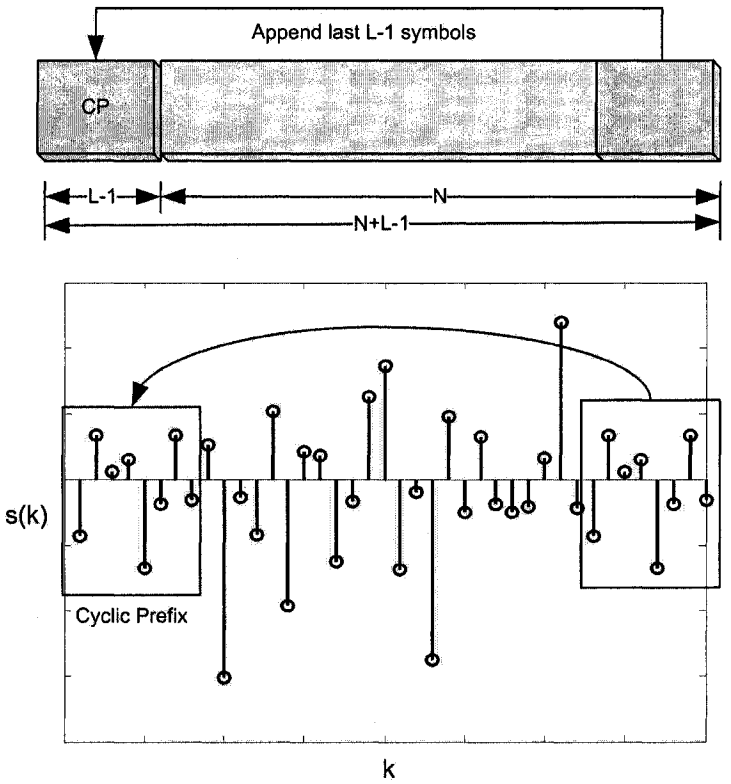

Fig. 2.11 Cyclic Prefix Insertion.

additive noise $\eta(n)$:

$$\begin{aligned} y(n) &= g(n) * \tilde{x}(n) + \eta(n) \\ &= \sum_{m=0}^{L-1} g(m)\tilde{x}(n-m) + \eta(n), \quad 0 \leq n \leq N-1. \end{aligned} \tag{2.20}$$

Using the fact that $\tilde{x}(n) = x(n)_N$ for $-L+1 \leq n \leq N-1$, we can replace the linear convolution with a circular convolution:

$$y(n) = \sum_{m=0}^{L-1} g(m)x(n-m)_N + \eta(n), \quad 0 \leq n \leq N-1. \tag{2.21}$$

Removing the first $L-1$ redundant samples and taking an N-point DFT of both sides of

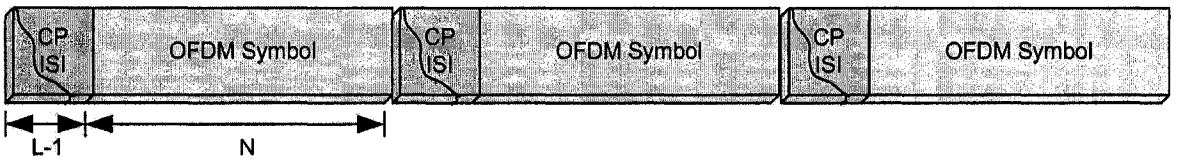

Fig. 2.12 ISI between OFDM symbols.

(2.21), the channel output for the kth subcarrier can be written as

$$\hat{s}(k) = h(k)s(k) + n(k), \quad 0 \leq k \leq N-1, \tag{2.22}$$

where

$$h(k) = \sum_{n=0}^{L-1} g(n)e^{-\frac{j2\pi kn}{N}} \tag{2.23}$$

is the sampled frequency response of the channel and $n(k)$ is an additive noise, which is modeled as a ZMCSCG random variable with variance N_0. From (2.22), it can be found that the broadband multipath fading channel is effectively decoupled into N parallel narrowband flat fading channels using the CP and IFFT/FFT operations [26]. Therefore, the CP insertion preserves orthogonality between subcarriers, avoiding ICI. The effects of flat fading can be easily removed by a simple single tap equalizer. This in turn would require simpler receiver designs than those for frequency selective channels.

Assuming that the complex symbol stream are divided into blocks of size N and the channel length is L, the channel output corrupted by ISI between successive OFDM symbols is illustrated in Fig. 2.12. If the length of CP is longer than that of the sampled channel impulse response, we can recover the original OFDM symbol by just discarding the corrupted samples, corresponding to the CP, which in turn completely eliminates ISI caused by the previous symbols.

Elimination of ICI and ISI comes at a price. The insertion of CP between the OFDM symbols introduces some additional overhead and extra transmit energy on the system. When the length of CP is $L-1$, the overhead is $(L-1)/N$ and the data rate reduction is $N/(N+L-1)$.

2.3 Chapter Summary

The first part of this chapter presented an overview of collaborative beamforming using random arrays. In particular, we investigated the average beampattern and directivity of random arrays, and the achievable beamforming gain through collaborative beamforming in the presence of synchronization errors. In the second part of this chapter, we discussed basic principles of OFDM, including orthogonality of carriers, basic baseband OFDM transceivers, and CP insertion to eliminate ISI and maintain orthogonality between subcarriers.

Chapter 3

Robust Beamforming for Collaborative MIMO-OFDM Wireless Systems

In an energy-constrained network, collaborative beamforming is a powerful technique to increase communication efficiency as presented in Chapter 2. In order to achieve high performance, however, collaborative beamforming requires accurate knowledge of CSI at the transmitter side, which is rarely available in practice. A robust transmitter design based on partial CSI is therefore required to mitigate the effects of channel mismatches.

This chapter aims to provide a beamforming scheme that is robust against CSI errors for collaborative MIMO-OFDM wireless systems. Section 3.1 presents the system model for OFDM wireless systems based on collaborative transmission and system block diagrams. In Section 3.2, a robust OFDM beamformer that achieves the best performance under the worst-case channel mismatch by maximizing the minimum received SNR within a predefined uncertainty region is derived based on the max-min robust design approach of [17].

3.1 System Model

3.1.1 Single Node Transmission

We consider an N-subcarrier OFDM system where one symbol is transmitted with one subcarrier. The block diagram of a baseband OFDM system for transmission from a single

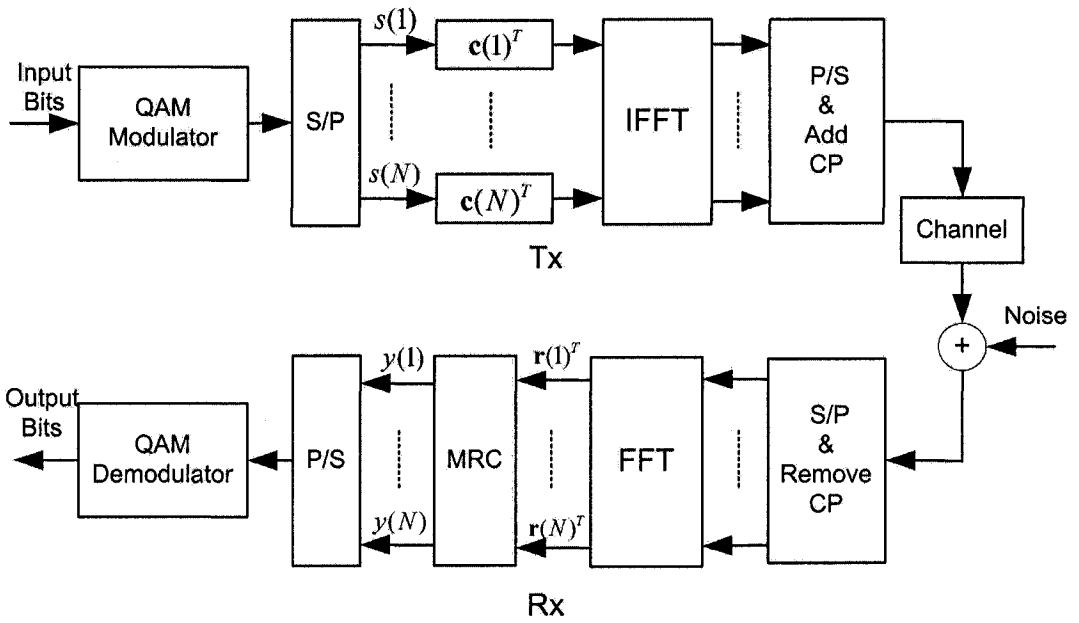

Fig. 3.1 Block diagram of a baseband OFDM system with transmit vectors $\mathbf{c}(k)$.

node equipped with one antenna is shown in Fig. 3.1. At the kth subcarrier frequency, the complex symbol $s(k)$ is first modulated by the transmit vector (precoder) $\mathbf{c}(k) = [c_1(k), c_2(k), \ldots, c_P(k)]^T$ of length P. After the IFFT and CP insertion, OFDM symbols are transmitted into a radio channel. Note that one OFDM symbol is sent over P time slots due to the spreading. Assuming that the length of CP is longer than that of the delay spread of the channel, the FFT output at the kth subcarrier can be expressed as

$$\mathbf{r}(k) = \mathbf{c}(k)h(k)s(k) + \mathbf{n}(k), \quad 1 \leq k \leq N \tag{3.1}$$

where $h(k)$ is the complex channel gain for subcarrier k as defined in (2.23), $\mathbf{n}(k)$ is the ZMCSCG noise vector with covariance matrix $N_0\mathbf{I}_P$. Assuming that the receiver has perfect knowledge of $\mathbf{c}(k)$ and $h(k)$, the output of the maximum ratio combiner (MRC) at the kth subcarrier is given by

$$\begin{aligned} y(k) &= (\mathbf{c}(k)h(k))^H \mathbf{r}(k) \\ &= \mathbf{c}^H(k)\mathbf{c}(k)|h(k)|^2 s(k) + h^*(k)\mathbf{c}^H(k)\mathbf{n}(k), \quad 1 \leq k \leq N. \end{aligned} \tag{3.2}$$

After the P/S conversion, the received bitstream can be estimated by the QAM demodulator.

3.1.2 Multiple Nodes Transmission

Now we consider an N-subcarrier OFDM based distributed wireless system consisting of a network of M_t nodes that transmits a common message to a distant receiver with M_r antennas. Assuming that each node is equipped with a single antenna as modeled in Fig. 3.1, a virtual MIMO-OFDM system can be used to model a cooperative communication system as illustrated in Fig. 3.2. In this thesis, we assume that all transmit nodes are perfectly synchronized with each other and data are shared *a priori* among all nodes in order to perform transmit beamforming toward direction of interest [1] At the kth subcarrier of the mth node, the complex message signal $s(k)$ is processed by the transmit vector $\mathbf{w}^{(m)}(k) = [w_1^{(m)}(k), w_2^{(m)}(k), \ldots, w_P^{(m)}(k)]^T$ of length P ($P \geq M_t$). Then, one symbol per carrier is transmitted over P time slots. Note that conditions on the length of the transmit vector will be discussed in more detail later. As in Section 3.1.1, we assume that the length of CP is longer than that of the delay spread of the channel. After the IFFT/FFT, the output of the jth receive antenna corrupted by additive noise at the kth subcarrier can be expressed as

$$\mathbf{r}_j(k) = \mathbf{W}(k)\mathbf{h}_j(k)s(k) + \mathbf{n}_j(k), \quad 1 \leq k \leq N, \quad 1 \leq j \leq M_r \tag{3.3}$$

where

$$\mathbf{W}(k) = [\mathbf{w}^{(1)}(k), \mathbf{w}^{(2)}(k), \ldots, \mathbf{w}^{(M_t)}(k)] \tag{3.4}$$

$$= \begin{bmatrix} w_1^{(1)}(k) & w_1^{(2)}(k) & \cdots & w_1^{(M_t)}(k) \\ w_2^{(1)}(k) & w_2^{(2)}(k) & \cdots & w_2^{(M_t)}(k) \\ \vdots & \vdots & \ddots & \vdots \\ w_P^{(1)}(k) & w_P^{(2)}(k) & \cdots & w_P^{(M_t)}(k) \end{bmatrix} \tag{3.5}$$

[1] In a pratical system, these conditions can be satisfied, *e.g.*, if dedicated communicaiton links are available between nodes.

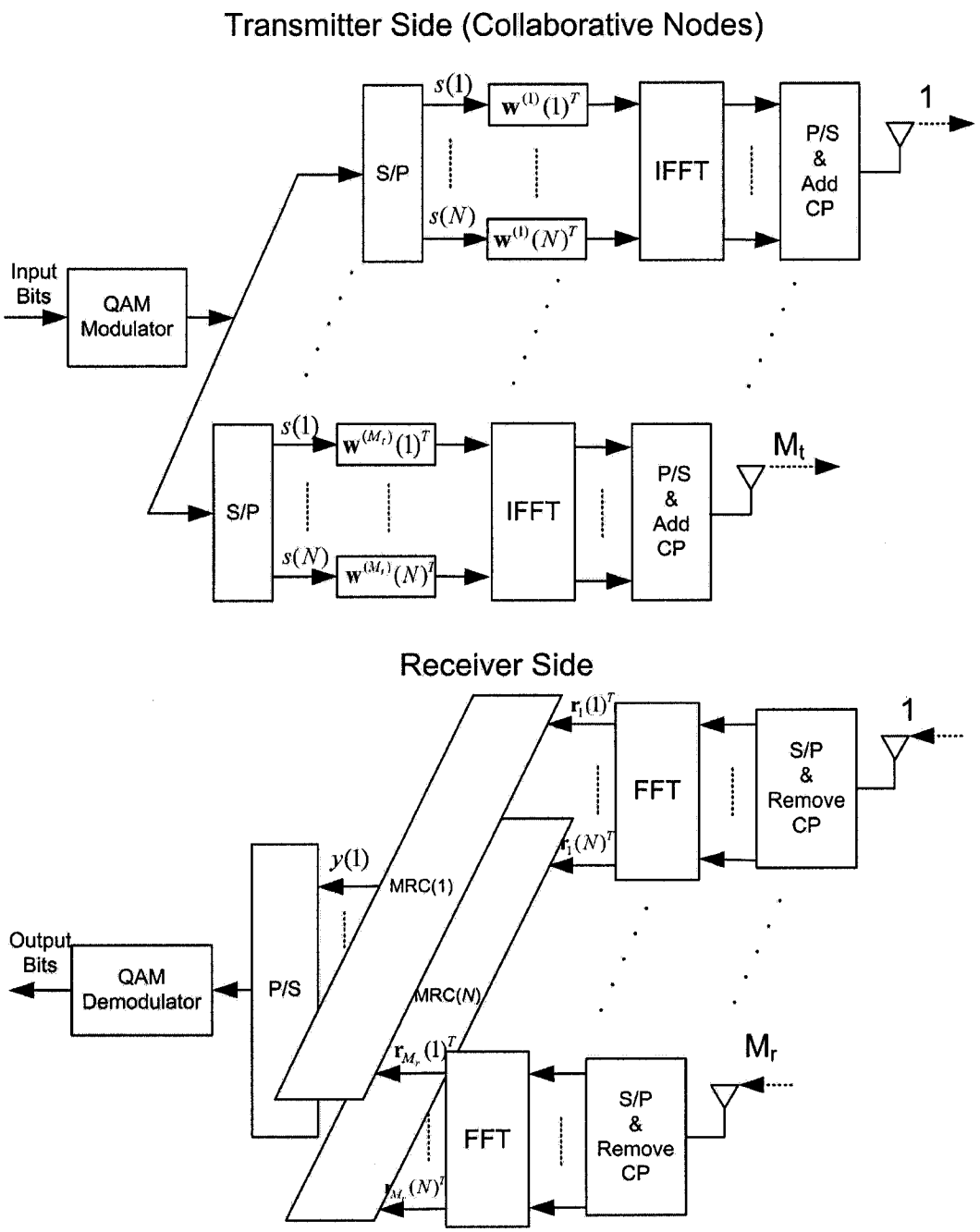

Fig. 3.2 Block diagram of a virtual MIMO-OFDM system with collaborative beamforming.

is the beamforming (or precoding) matrix and the entry $w_p^{(m)}(k)$ represents the pth transmit beamforming weight at the mth transmit node, $\mathbf{h}_j(k) = [h_j^{(1)}(k), h_j^{(2)}(k), \ldots, h_j^{(M_t)}(k)]^T$ is the frequency domain channel response vector and the entry $h_j^{(m)}(k)$ represents a complex gain at the jth receive antenna from the mth transmit node, $s(k)$ is the complex symbol, and $\mathbf{n}_j(k) = [n_j^{(1)}(k), n_j^{(2)}(k), \ldots, n_j^{(P)}(k)]^T$ is the ZMCSCG noise vector with covariance matrix $N_0\mathbf{I}_P$ at the jth receive antenna. Note that the rows of $\mathbf{W}(k)$ correspond to spatial beamforming vectors across M_t collaborative nodes during P time slots.

The beamforming matrix $\mathbf{W}(k)$ and the CSI $\mathbf{h}_j(k)$ are assumed to be perfectly known at the receiver side. Then, $\mathbf{g}_j(k) = \mathbf{W}(k)\mathbf{h}_j(k)$ is the combining vector at the jth receive antenna. The output of the MRC at the kth subcarrier for the jth receive antenna can be expressed as

$$\begin{aligned} y_j(k) &= \{\mathbf{g}_j(k)\}^H \mathbf{r}_j(k) \\ &= \mathbf{h}_j^H(k)\mathbf{W}^H(k)\mathbf{W}(k)\mathbf{h}_j(k)s(k) + \mathbf{h}_j^H(k)\mathbf{W}^H(k)\mathbf{n}_j(k). \end{aligned} \tag{3.6}$$

The SNR for subcarrier k at the jth receive antenna can be written as

$$\begin{aligned} \mathrm{SNR}_j(k) &= \frac{E\left\{|\mathbf{h}_j^H(k)\mathbf{W}^H(k)\mathbf{W}(k)\mathbf{h}_j(k)s(k)|^2\right\}}{E\left\{|\mathbf{h}_j^H(k)\mathbf{W}^H(k)\mathbf{n}_j(k)|^2\right\}} \\ &= \frac{\mathbf{h}_j^H(k)\mathbf{W}^H(k)\mathbf{W}(k)\mathbf{h}_j(k)E\left\{s(k)s^*(k)\right\}\mathbf{h}_j^H(k)\mathbf{W}^H(k)\mathbf{W}(k)\mathbf{h}_j(k)}{\mathbf{h}_j^H(k)\mathbf{W}^H(k)E\left\{\mathbf{n}_j(k)\mathbf{n}_j^H(k)\right\}\mathbf{W}(k)\mathbf{h}_j(k)} \\ &= \frac{E_s}{N_0}\gamma_j(k) \end{aligned} \tag{3.7}$$

where

$$\gamma_j(k) = \mathbf{h}_j^H(k)\mathbf{W}^H(k)\mathbf{W}(k)\mathbf{h}_j(k) \tag{3.8}$$

is the effective channel gain and $E_s = E\{|s(k)|^2\}$ is the average symbol energy. With M_r

receive antennas, the combined signal at subcarrier k is given by

$$\begin{aligned} y(k) &= \sum_{j=1}^{M_r} \mathbf{g}_j^H(k)\mathbf{r}_j(k) \\ &= \mathrm{tr}\left\{\mathbf{G}^H(k)\mathbf{R}(k)\right\} \\ &= \sum_{j=1}^{M_r} \left\{\mathbf{h}_j^H(k)\mathbf{W}^H(k)\mathbf{W}(k)\mathbf{h}_j(k)s(k) + \mathbf{h}_j^H(k)\mathbf{W}^H(k)\mathbf{n}_j(k)\right\} \end{aligned} \tag{3.9}$$

where $\mathbf{G}(k) = [\mathbf{g}_1(k), \mathbf{g}_2(k), \ldots, \mathbf{g}_{M_r}(k)]$ is the $P \times M_r$ combining matrix and $\mathbf{R}(k) = [\mathbf{r}_1(k), \mathbf{r}_2(k), \ldots, \mathbf{r}_{M_r}(k)]$ is the $P \times M_r$ received signal matrix. Finally, the overall SNR for subcarrier k can be written as

$$\begin{aligned} \mathrm{SNR}(k) &= \frac{E\left\{\left|\sum_{j=1}^{M_r} \mathbf{h}_j^H(k)\mathbf{W}^H(k)\mathbf{W}(k)\mathbf{h}_j(k)s(k)\right|^2\right\}}{E\left\{\left|\sum_{j=1}^{M_r} \mathbf{h}_j^H(k)\mathbf{W}^H(k)\mathbf{n}_j(k)\right|^2\right\}} \\ &= \frac{E_s}{N_0}\Gamma(k) \end{aligned} \tag{3.10}$$

where

$$\begin{aligned} \Gamma(k) &= \sum_{j=1}^{M_r} \mathbf{h}_j^H(k)\mathbf{W}^H(k)\mathbf{W}(k)\mathbf{h}_j(k) \\ &= \mathrm{tr}\left\{\mathbf{H}^H(k)\mathbf{W}^H(k)\mathbf{W}(k)\mathbf{H}(k)\right\} \end{aligned} \tag{3.11}$$

is the overall effective channel gain (OECG) and $\mathbf{H}(k) = [\mathbf{h}_1(k), \mathbf{h}_2(k), \ldots, \mathbf{h}_{M_r}(k)]$ is the $M_t \times M_r$ channel matrix. In deriving (3.10), we assume that $E\left\{\mathbf{n}_j(k)\mathbf{n}_l^H(k)\right\} = \delta_{jl}N_0\mathbf{I}_P$.

Assuming unit energy symbols $E_s = E\{|s(k)|^2\} = 1$, the average power of the transmitted signal at the kth subcarrier can be expressed as

$$E\left\{\|\mathbf{W}(k)s(k)\|^2\right\} = \|\mathbf{W}(k)\|_F^2 = \mathrm{tr}\left\{\mathbf{W}^H(k)\mathbf{W}(k)\right\}. \tag{3.12}$$

The ultimate parameter for evaluating the quality of communication systems is their error probability, *e.g.*, symbol error probability (SEP) or bit error probability (BEP), which can be estimated by the BER and SER measurement. Under the zero-mean Gaussian noise

assumption, the SEP for the kth subcarrier $P_e(k)$ can be expressed as [19,27]

$$P_e(k) = \mathcal{Q}\left(\sqrt{k_m \mathrm{SNR}(k)}\right) \tag{3.13}$$

where k_m is a constellation-specific constant and $\mathcal{Q}$ is the $\mathcal{Q}$-function defined by $\mathcal{Q}(x) = \left(1/\sqrt{2\pi}\right) \int_x^\infty e^{-u^2/2} du$. By averaging (3.13) over all N subcarriers, the effective SEP can be obtained as [20]

$$P_{e,\mathrm{eff}} = \frac{1}{N} \sum_{k=1}^{N} P_e(k). \tag{3.14}$$

Using the Chernoff bound [27] $\mathcal{Q}(x) \leq (1/2)e^{-x^2/2}$, we can find an upper bound on the SEP for the kth subcarrier in (3.13) as

$$P_e(k) \leq P_{e,\mathrm{bound}}(k) \triangleq \frac{1}{2} e^{-\frac{k_m \mathrm{SNR}(k)}{2}}. \tag{3.15}$$

The bound (3.15) is a deceasing function of the SNR(k). Thus, maximizing the SNR is equivalent to minimizing the SEP. In the following section, we present a robust beamformer that maximizes the worst-case received SNR.

3.2 Robust Beamforming for Collaborative Transmission

In Section 3.1, the system model for collaborative MIMO-OFDM communication systems with transmit beamforming and receive combining was formulated. This section aims at designing the beamforming matrix $\mathbf{W}(k)$ that provides the best SNR performance in worst-case scenario by maximizing the minimum received SNR within a predefined uncertainty region at each OFDM subcarriers. The underlying approach is based on [17]. In the following, the cost function including the channel uncertainty (partial CSI) and the corresponding analytical closed-form solution are presented.

3.2.1 Cost Function

In practice, perfect CSI, *i.e.*, knowledge of $\{\mathbf{H}(k)\}_{k=1}^N$, is not available at the transmitters due to the time varying channels caused by the movements of collaborating nodes and surrounding objects, channel estimation errors, and channel feedback delay. Hence, the

design of the beamforming matrices $\{\mathbf{W}(k)\}_{k=1}^{N}$ must be based on the estimated CSI at the transmitters. The *true* channel matrix for the kth subcarrier can be expressed as

$$\mathbf{H}(k) = \hat{\mathbf{H}}(k) + \mathbf{E}(k), \quad 1 \leq k \leq N \tag{3.16}$$

where

$$\hat{\mathbf{H}}(k) = [\hat{\mathbf{h}}_1(k), \hat{\mathbf{h}}_2(k), \ldots, \hat{\mathbf{h}}_{M_r}(k)] \tag{3.17}$$

$$\mathbf{E}(k) = [\mathbf{e}_1(k), \mathbf{e}_2(k), \ldots, \mathbf{e}_{M_r}(k)] \tag{3.18}$$

are the *presumed* channel matrix at the transmitters and the unknown channel estimation error matrix, respectively. In this work, the norm of the error matrix at each frequency is assumed to be bounded by some known constant $\varepsilon(k) > 0$:

$$\|\mathbf{E}(k)\|_F \leq \varepsilon(k). \tag{3.19}$$

In practice, the value of the constant $\varepsilon(k)$ is provided by the user on the basis of available knowledge about the channel estimation quality. Therefore, the uncertainty region for the kth subcarrier can be modeled as a sphere of radius $\varepsilon(k)$ centered at the presumed channel $\hat{\mathbf{H}}(k)$. Fig. 3.3 illustrates a two-dimensional representation of the uncertainty region for subcarrier k according to

$$\mathcal{R}_k = \{\mathbf{E}(k) : \|\mathbf{E}(k)\|_F \leq \varepsilon(k)\}. \tag{3.20}$$

Substituting (3.16) into (3.12), the OECG can be rewritten as

$$\Gamma(k) = \mathrm{tr}\left\{(\hat{\mathbf{H}}(k) + \mathbf{E}(k))^H \mathbf{W}^H(k)\mathbf{W}(k)(\hat{\mathbf{H}}(k) + \mathbf{E}(k))\right\}. \tag{3.21}$$

Considering (3.21) as a system performance criterion and the max-min robust design approach of [17], the beamforming matrix for the kth subcarrier can be obtained by maximizing the minimum (worst performance over all channel errors) of the OECG of that

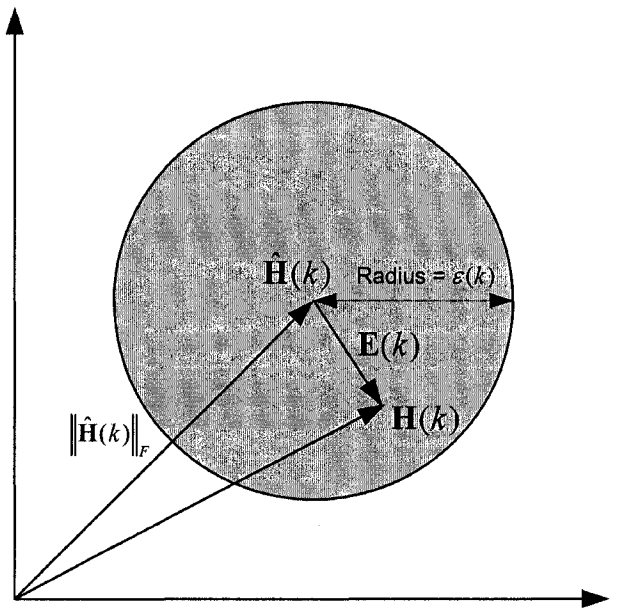

Fig. 3.3 A two-dimensional representation of the uncertainty region for subcarrier k.

subcarrier subject to a transmit power constraint, *i.e.*,

$$\begin{aligned} &\underset{\mathbf{W}(k)}{\text{maximize}} \quad \min_{\mathbf{E}(k)\in\mathcal{R}_k} \Gamma(k) \\ &\text{subject to} \quad \text{tr}\{\mathbf{W}^H(k)\mathbf{W}(k)\} \leq p(k) \end{aligned} \tag{3.22}$$

where $p(k)$ represents the maximum available transmit power at the kth subcarrier. Note that a summation of the power constraint $p(k)$ for all k represents the global transmit power available at the collaborative nodes. Power allocation strategies to distribute the global transmit power to OFDM subcarriers will be discussed in Chapter 4.

3.2.2 Eigen Beamforming

In order to simplify the cost function $\Gamma(k)$ in (3.22), the positive semi-definite matrices $\mathbf{W}^H(k)\mathbf{W}(k)$ and $\hat{\mathbf{H}}(k)\hat{\mathbf{H}}^H(k)$ are expressed in terms of their eigenvalue decomposition

(EVD) as

$$\mathbf{W}^H(k)\mathbf{W}(k) = \mathbf{U}_w(k)\mathbf{D}_w(k)\mathbf{U}_w^H(k) \tag{3.23}$$

$$\hat{\mathbf{H}}(k)\hat{\mathbf{H}}^H(k) = \mathbf{U}_{\hat{h}}(k)\mathbf{D}_{\hat{h}}(k)\mathbf{U}_{\hat{h}}^H(k) \tag{3.24}$$

$$\mathbf{D}_w(k) = \text{diag}(d_{w_1}(k), \cdots, d_{w_{M_t}}(k)) \tag{3.25}$$

$$\mathbf{D}_{\hat{h}}(k) = \text{diag}(d_{\hat{h}_1}(k), \cdots, d_{\hat{h}_{M_t}}(k)) \tag{3.26}$$

where $\mathbf{U}_w(k) = [\mathbf{u}_{w_1}(k), \mathbf{u}_{w_2}(k), \ldots, \mathbf{u}_{w_{M_t}}(k)]$ and $\mathbf{U}_{\hat{h}}(k) = [\mathbf{u}_{\hat{h}_1}(k), \mathbf{u}_{\hat{h}_2}(k), \ldots, \mathbf{u}_{\hat{h}_{M_t}}(k)]$ are the unitary matrices whose columns are the orthonormal eigenvectors of $\mathbf{W}^H(k)\mathbf{W}(k)$ and $\hat{\mathbf{H}}(k)\hat{\mathbf{H}}^H(k)$, respectively, and $\mathbf{D}_w(k)$ and $\mathbf{D}_{\hat{h}}(k)$ contain the corresponding eigenvalues sorted in non-increasing order, *i.e.*, $d_{w_1}(k) \geq d_{w_2}(k) \geq \cdots \geq d_{w_{M_t}}(k)$ and $d_{\hat{h}_1}(k) \geq d_{\hat{h}_2}(k) \geq \cdots \geq d_{\hat{h}_{M_t}}(k)$. Then, the beamforming matrix for the kth subcarrier can be expressed as

$$\mathbf{W}(k) = \mathbf{\Phi}(k)\mathbf{D}_w^{1/2}(k)\mathbf{U}_w^H(k) \tag{3.27}$$

where $\mathbf{\Phi}(k)$ is a $P \times M_t$ arbitrary maxtix whose columns are orthonormal, *i.e.*, $\mathbf{\Phi}^H(k)\mathbf{\Phi}(k) = \mathbf{I}_{M_t}$ [14]. If $P < M_t$, the matrix $\mathbf{W}^H(k)\mathbf{W}(k)$ will lose rank and have some zero eigenvalues, resulting in a loss of diversity gain. However, if $P > M_t$, the system does not gain anything and introduces an additional data rate loss. Thus, the length P should be chosen to be equal to M_t. Note that replacing the arbitrary matrix $\mathbf{\Phi}(k)$ with orthogonal space-time block codes (STBC) can compensate for the data rate loss incurred during spreading [14, 28].

As shown in [17, 18, 20], the optimum transmit beamformer having perfect channel knowledge only utilizes the maximum eigenmode of the channel correlation matrix. In the case with imperfect channel knowledge, however, it is shown in [17, 18, 29] that the robust transmit beamformer takes full advantage of the available estimated eigenmodes of the channel correlation matrix. In this thesis, we consider eigen beamforming in which symbols are transmitted along the eigenvectors of the presumed channel correlation matrices

$\{\hat{\mathbf{H}}(k)\hat{\mathbf{H}}^H(k)\}_{k=1}^N$, *i.e.*, $\mathbf{U}_w(k) = \mathbf{U}_{\hat{h}}(k)$. The beamforming matrix (3.27) can be written as

$$\mathbf{W}(k) = \mathbf{\Phi}(k)\mathbf{D}_w^{1/2}(k)\mathbf{U}_{\hat{h}}^H(k) \tag{3.28}$$

$$= \mathbf{\Phi}(k) \begin{bmatrix} \sqrt{d_{w_1}(k)} & 0 & \cdots & 0 \\ 0 & \sqrt{d_{w_2}(k)} & \ddots & \vdots \\ \vdots & \ddots & \ddots & 0 \\ 0 & \cdots & 0 & \sqrt{d_{w_{M_t}}(k)} \end{bmatrix} \begin{bmatrix} \mathbf{u}_{\hat{h}_1}^H(k) \\ \mathbf{u}_{\hat{h}_2}^H(k) \\ \vdots \\ \mathbf{u}_{\hat{h}_{M_t}}^H(k) \end{bmatrix}. \tag{3.29}$$

At each OFDM subcarrier, the robust beamformer collaboratively forms eigenbeams along the eigenvectors of the estimated channel correlation matrix $\mathbf{U}_{\hat{h}}(k)$ and distributes the available transmit power across those eigenbeams $\mathbf{D}_w^{1/2}(k)$. Then, the weighted eigenbeams (eigenvectors) are projected onto the basis vectors $\mathbf{\Phi}(k)$.

An analytical solution to the max-min optimization problem (3.22) can be obtained by first solving the inner minimization problem and then solving the outer maximization problem. The closed-form solution of the optimization problem is presented in the following subsections.

3.2.3 Worst-Case Error

The first step is to determine the worst-case error matrix which produces the minimum of the cost function. From (3.22), the inner minimization problem can be written as

$$\begin{aligned} &\underset{\mathbf{E}(k)}{\text{minimize}} \quad \Gamma(k) \\ &\text{subject to} \quad \|\mathbf{E}(k)\|_F^2 \leq \varepsilon^2(k) \end{aligned} \tag{3.30}$$

where the expression for $\Gamma(k)$ is available from (3.21). Using the Lagrange multiplier method, the Lagrangian for the inner minimization problem can be written as

$$\mathcal{L}(k) = \Gamma(k) + \lambda(k)\left(\|\mathbf{E}(k)\|_F^2 - \varepsilon^2(k)\right) \tag{3.31}$$

where $\lambda(k)$ is the Lagrange multiplier. Differentiating[2] (3.31) with respect to $\mathbf{E}^*(k)$, we have that [30]

$$\begin{aligned}\frac{\partial \mathcal{L}(k)}{\partial \mathbf{E}^*(k)} &= \frac{\partial \{\Gamma(k)\}}{\partial \mathbf{E}^*(k)} + \lambda(k)\frac{\partial \left\{\|\mathbf{E}(k)\|_F^2 - \varepsilon^2(k)\right\}}{\partial \mathbf{E}^*(k)} \\ &= \mathbf{W}^H(k)\mathbf{W}(k)\hat{\mathbf{H}}(k) + \mathbf{W}^H(k)\mathbf{W}(k)\mathbf{E}(k) + \lambda(k)\mathbf{E}(k). \end{aligned} \tag{3.32}$$

Equating (3.32) to zero and solving for $\mathbf{E}(k)$, it is found that the minimum of $\Gamma(k)$ (3.21) is achieved at

$$\mathbf{E}_{\min}(k) = -\left(\mathbf{W}^H(k)\mathbf{W}(k) + \lambda(k)\mathbf{I}\right)^{-1}\mathbf{W}^H(k)\mathbf{W}(k)\hat{\mathbf{H}}(k). \tag{3.33}$$

Using the EVD and the structural constraint (3.28), the worst-case error matrix $\mathbf{E}_{\min}(k)$ can be rewritten as

$$\mathbf{E}_{\min}(k) = -\mathbf{U}_{\hat{h}}(k)\text{diag}\left\{\frac{d_{w_i}(k)}{d_{w_i}(k)+\lambda(k)}\right\}\mathbf{U}_{\hat{h}}{}^H(k)\hat{\mathbf{H}}(k) \tag{3.34}$$

where the Lagrange multiplier $\lambda(k)$ satisfies

$$\begin{aligned}\varepsilon^2(k) &= \text{tr}\left\{\mathbf{D}_{\hat{h}}(k)\text{diag}\left\{\left(\frac{d_{w_i}(k)}{d_{w_i}(k)+\lambda(k)}\right)^2\right\}\right\} \\ &= \sum_{i=1}^{M_t} d_{\hat{h}_i}(k)\left(\frac{d_{w_i}(k)}{d_{w_i}(k)+\lambda(k)}\right)^2. \end{aligned} \tag{3.35}$$

Note that (3.35) is obtained by substituting (3.34) in the constraint $\|\mathbf{E}(k)\|_F^2 = \varepsilon^2(k)$. Substituting (3.34) into (3.21), the worst-case (minimum) OECG can be expressed as

$$\Gamma_{\min}(k) = \sum_{i=1}^{M_t} d_{\hat{h}_i}(k)\left[d_{w_i}(k)\left(\frac{\lambda(k)}{d_{w_i}(k)+\lambda(k)}\right)^2\right] \tag{3.36}$$

where $\lambda(k)$ also satisfies (3.35). The determination of $\lambda(k)$ via (3.35) is considered as part of the outer optimimizaiton problem below where the determination of $d_{w_i}(k)$ is considered.

[2] In this thesis, we adapt the framework of [30] regarding differentiation of a real cost function with respect to complex parameters. This reference also contains several useful results that are used in the derivation below.

3.2.4 Robust Power Loading Across Eigenmodes

Once we determine the worst-case error matrix (3.34) and the corresponding worst-case OECG (3.36), we can rewrite the optimization problem (3.22) as

$$\begin{aligned} \underset{d_{w_i}(k)}{\text{maximize}} \quad & \Gamma_{\min}(k) \\ \text{subject to} \quad & \sum_{i=1}^{M_t} d_{w_i}(k) \leq p(k) \\ & d_{w_i}(k) \geq 0, \quad \forall i \end{aligned} \tag{3.37}$$

where

$$\sum_{i=1}^{M_t} d_{w_i}(k) = \text{tr}\{\mathbf{W}^H(k)\mathbf{W}(k)\} = \text{tr}\{\mathbf{D}_w(k)\}. \tag{3.38}$$

The solution to this outer maximization (3.37) can be obtained using the Karush-Kuhn-Tucker (KKT) optimality conditions by minimizing the Lagrangian [31]:

$$\mathcal{L}(k) = -\Gamma_{\min}(k) + v(k)\left(\sum_{i=1}^{M_t} d_{w_i}(k) - p(k)\right) - \sum_{i=1}^{M_t} \mu_i(k) d_{w_i}(k) \tag{3.39}$$

where $v(k)$ and $\mu_i(k)$ are the Lagrange multipliers. Then, differentiating (3.39) with respect to $d_{w_i}(k)$ yields

$$\frac{\partial \mathcal{L}(k)}{\partial d_{w_i}(k)} = -d_{\hat{h}_i}(k)\left(\frac{\lambda(k)}{\lambda(k) + d_{w_i}(k)}\right)^2 + v(k) - \mu_i(k). \tag{3.40}$$

The KKT optimality conditions are given by ($i = 1, \ldots, M_t$)

$$d_{w_i}(k) \geq 0, \quad \sum_{i=1}^{M_t} d_{w_i}(k) = p(k), \tag{3.41}$$

$$\mu_i(k) \geq 0, \tag{3.42}$$

$$v(k) - \mu_i(k) - d_{\hat{h}_i}(k)\left(\frac{\lambda(k)}{\lambda(k) + d_{w_i}(k)}\right)^2 = 0, \tag{3.43}$$

$$\mu_i(k) d_{w_i}(k) = 0. \tag{3.44}$$

Eliminating the Lagrange multiplier $\mu_i(k)$, the KKT optimality conditions are reduced to

$$d_{w_i}(k) \geq 0, \quad \sum_{i=1}^{M_t} d_{w_i}(k) = p(k), \tag{3.45}$$

$$v(k) - d_{\hat{h}_i}(k) \left(\frac{\lambda(k)}{\lambda(k) + d_{w_i}(k)} \right)^2 \geq 0, \tag{3.46}$$

$$\left[v(k) - d_{\hat{h}_i}(k) \left(\frac{\lambda(k)}{\lambda(k) + d_{w_i}(k)} \right)^2 \right] d_{w_i}(k) = 0. \tag{3.47}$$

From the KKT optimality conditions, the optimum power loading solution can be found as follows: If $v(k) < d_{\hat{h}_i}(k)$, then $\frac{\lambda(k)}{\lambda(k)+d_{w_i}(k)} < 1$ from (3.46), which implies that $d_{w_i}(k) > 0$. Therefore, we have that $v(k) = d_{\hat{h}_i}(k) \left(\frac{\lambda(k)}{\lambda(k)+d_{w_i}(k)} \right)^2$ from (3.47). Solving for $d_{w_i}(k)$, $d_{w_i}(k) = \lambda(k) \left(\sqrt{d_{\hat{h}_i}(k)/v(k)} - 1 \right)$ if $v(k) < d_{\hat{h}_i}(k)$. If $v(k) \geq d_{\hat{h}_i}(k)$ and $d_{w_i}(k) > 0$, then $v(k) > d_{\hat{h}_i}(k) \left(\frac{\lambda(k)}{\lambda(k)+d_{w_i}(k)} \right)^2$ which violates (3.47). Therefore, $d_{w_i}(k) = 0$ if $v(k) \geq d_{\hat{h}_i}(k)$. Equivalently, the solution can be expressed as

$$\begin{aligned} d_{w_i}(k) &= \begin{cases} \lambda(k) \left(\sqrt{\frac{d_{\hat{h}_i}(k)}{v(k)}} - 1 \right), & v(k) < d_{\hat{h}_i}(k) \\ 0, & v(k) \geq d_{\hat{h}_i}(k) \end{cases} \\ &= \frac{\lambda(k)}{\sqrt{v(k)}} \left(\sqrt{d_{\hat{h}_i}(k)} - \sqrt{v(k)} \right)^+ \end{aligned} \tag{3.48}$$

where the constants $\lambda(k)$ and $v(k)$ are chosen such that the total transmit power for a given subcarrier k is satisfied, *i.e.*,

$$\sum_{i=1}^{M_t} d_{w_i}(k) = p(k) \tag{3.49}$$

and that (3.35) is also satisfied. Fig. 3.4 shows a pictorial representation of optimal power loading across eigenmodes. Interestingly, the optimal power loading solution can be interpreted as a form of water-filling. We can think of $\sqrt{v}(k)$ as a water-level and the shaded area in Fig. 3.4 as the total amount of transmit power allocated to the kth subcarrier.

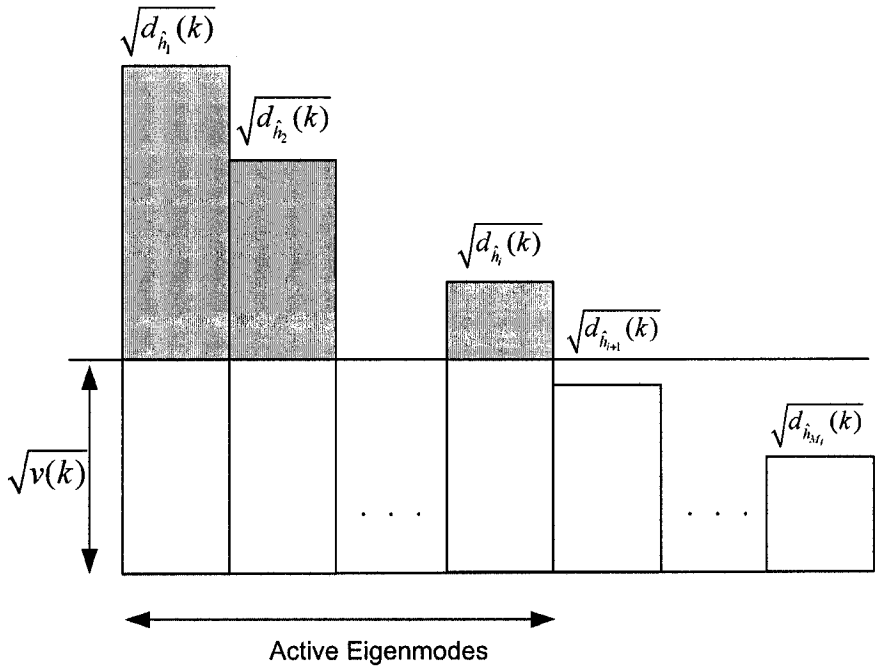

Fig. 3.4 A pictorial representation of optimal power loading across eigenmodes.

Letting $n(k) \in \{1, 2, \cdots, M_t\}$ be the number of the active eigenmodes for the kth subcarrier and substituting (3.48) into (3.35), we have the following second order equation in $\sqrt{v(k)}$:

$$\varepsilon^2(k) = \sum_{i=1}^{n(k)} \left(\sqrt{d_{\hat{h}_i}(k)} - \sqrt{v(k)} \right)^2 \tag{3.50}$$

$$= n(k)v(k) - \left(2 \sum_{i=1}^{n(k)} \sqrt{d_{\hat{h}_i}(k)} \right) \sqrt{v(k)} + \sum_{i=1}^{n(k)} d_{\hat{h}_i}(k). \tag{3.51}$$

For a given $n(k)$, the smallest root[3] of (3.51) is given by

$$v_{\min}(k) = \left[\frac{\alpha_n(k) - \sqrt{\alpha_n^2(k) + n(k)\left(\varepsilon^2(k) - \beta_n(k)\right)}}{n(k)} \right]^2 \tag{3.52}$$

[3]The largest root may result in $d_{w_i}(k) = 0$ for $i = \{1, \ldots, M_t\}$. See [17] for technical details related to this issue.

where

$$\alpha_n(k) = \sum_{i=1}^{n(k)} \sqrt{d_{\hat{h}_i}(k)}, \quad \beta_n(k) = \sum_{i=1}^{n(k)} d_{\hat{h}_i}(k). \tag{3.53}$$

By a simple finite iteration, we can always determine the value of $n(k)$ for which $d_{\hat{h}_{n(k)+1}}(k) \leq v_{\min}(k) < d_{\hat{h}_{n(k)}}(k)$ and $d_{\hat{h}_{M_t+1}}(k) = 0$. With the value of $n(k)$, we have $v(k) = v_{\min}(k)$. Then, $\lambda(k)$ [4] can be found by substituting (3.48) into the power constraint (3.49):

$$\sum_{i=1}^{n(k)} \left(\sqrt{\frac{d_{\hat{h}_i}(k)}{v(k)}} - 1 \right) = \frac{p(k)}{\lambda(k)}. \tag{3.54}$$

Lastly, $d_{w_i}(k)$ is obtained using (3.48).

Since $v(k)$ is inversely proportional to the size of the uncertainty region $\varepsilon(k)$ as in (3.50), the robust beamformer tends to use more eigenmodes to transmit data as $\varepsilon(k)$ increases. The robust beamformer takes full advantage of the available estimated eigenmodes of the channel and distributes the total transmit power across the eigenmodes in a water-filling fashion. In contrast, the nonrobust beamformer ($\varepsilon(k) = 0$) uses only the maximum eigenmode. A similar closed-form solution using convex optimization theory is found in [29].

The pseudo-code for computing a robust beamforming matrix at the kth subcarrier is given in Table 3.1.

3.2.5 Analysis of the Worst-Case OECG

Consider equal power loading across eigenmodes ($d_{w_i}(k) \equiv d_w(k), \forall i$). The corresponding worst-case OECG (3.36) can be expressed as

$$\Gamma_{\min}(k)|_{\text{equal}} = \left[d_w(k) \left(\frac{\lambda(k)}{d_w(k) + \lambda(k)} \right)^2 \right] \xi(k) \tag{3.55}$$

where $\lambda(k)$ satisfies

$$\varepsilon^2(k) = \left(\frac{d_w(k)}{d_w(k) + \lambda(k)} \right)^2 \xi(k) \tag{3.56}$$

[4] The same Lagrange multiplier $\lambda(k)$ as in (3.35)

Table 3.1 The pseudo-code for computing a robust beamforming matrix

1. Compute the samallest root $v_{\min}(k)$ using (3.52).
2. Determine the value of $n(k)$ for which $d_{\hat{h}_{n(k)+1}}(k) \leq v_{\min}(k) < d_{\hat{h}_{n(k)}}(k)$ and $d_{\hat{h}_{M_t+1}}(k) = 0$.
3. Determine the Lagrange multiplier $\lambda(k)$ using (3.35).
4. Compute robust power loading $d_{w_i}(k)$ using (3.48).
5. The robust beamforming matrix is obtained by $\mathbf{W}(k) = \mathbf{\Phi}(k)\mathbf{D}_w^{1/2}(k)\mathbf{U}_w^H(k)$.

and

$$\xi(k) = \sum_{i=1}^{M_t} d_{\hat{h}_i}(k). \tag{3.57}$$

Solving for $\lambda(k)$, we have

$$\lambda(k) = \left(\frac{\sqrt{\xi(k)}}{\varepsilon(k)} - 1\right) d_w(k). \tag{3.58}$$

By substituting (3.58) into (3.55), the worst-case OECG for equal power loading is given by

$$\Gamma_{\min}(k)|_{\text{equal}} = \xi(k) d_w(k) \left(1 - \frac{\varepsilon(k)}{\sqrt{\xi(k)}}\right)^2. \tag{3.59}$$

Now consider one-directional loading, *i.e.*, $\mathbf{D}_w(k) = \text{diag}(d_{w_1}(k), 0, \cdots, 0)$. The worst-case OECG (3.36) can be written as

$$\Gamma_{\min}(k)|_{1-\text{D}} = \left[d_{w_1}(k) \left(\frac{\lambda(k)}{d_{w_1}(k) + \lambda(k)}\right)^2\right] d_{\hat{h}_1}(k) \tag{3.60}$$

where $\lambda(k)$ satisfies

$$\varepsilon^2(k) = \left(\frac{d_{w_1}(k)}{d_{w_1}(k) + \lambda(k)}\right)^2 d_{\hat{h}_1}(k). \tag{3.61}$$

From (3.61), $\lambda(k)$ is given by

$$\lambda(k) = \left(\frac{\sqrt{d_{\hat{h}_1}(k)}}{\varepsilon(k)} - 1\right) d_{w_1}(k). \tag{3.62}$$

By substituting (3.63) into (3.60), the worst-case OECG for one-directional loading is given by

$$\Gamma_{\min}(k)|_{1-\mathrm{D}} = d_{\hat{h}_1}(k) d_{w_1}(k) \left(1 - \frac{\varepsilon(k)}{\sqrt{d_{\hat{h}_1}(k)}}\right)^2 \tag{3.63}$$

After equating (3.59) and (3.63), the size of the uncertainty region $\varepsilon(k)$ that corresponds to the same worst-case OECGs is obtained as,

$$\varepsilon(k) = \frac{\sqrt{d_{\hat{h}_1}(k) d_{w_1}(k)} - \sqrt{\xi(k) d_w(k)}}{\sqrt{d_{w_1}(k)} - \sqrt{d_w(k)}}. \tag{3.64}$$

Assuming that eigenvalues of an estimated channel correlation matrix for subcarrier k are $\mathbf{d}_{\hat{h}}(k) = [0.6371, 0.3029, 0.0601]^T$, the worst-case OECGs for one-directional loading, equal power loading, and robust loading against the size of the uncertainty region are plotted in Fig. 3.5. It can be observed that robust power loading offers the best worst-case performance over equal power loading and one-directional loading as expected. As $\varepsilon(k)$ increases, equal power loading approaches robust power loading. The interception point of one-directional loading and equal power loading is found to be $\varepsilon(k) = 0.5225$ in this example. More simulation results will be presented in Chapter 5.

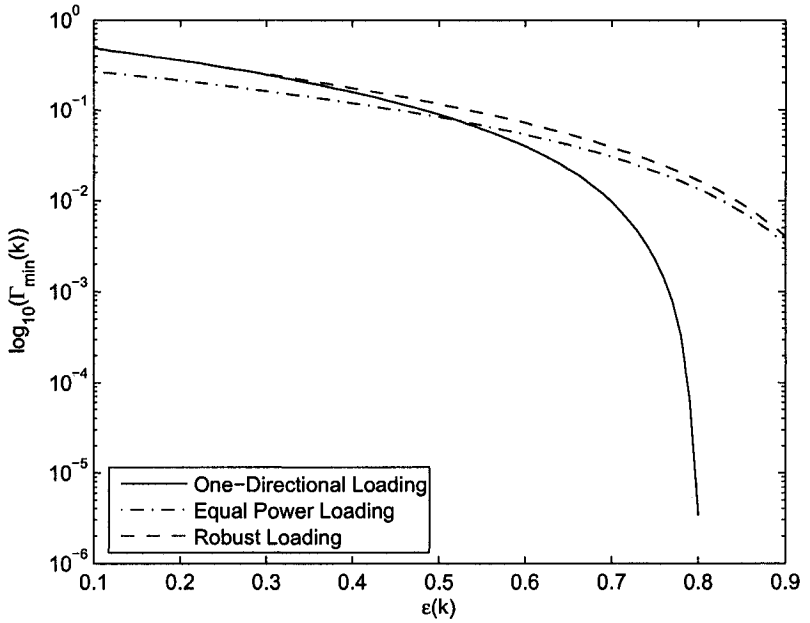

Fig. 3.5 Worst-case OECGs for one-directional loading, equal power loading, and robust loading against the size of the uncertainty region.

3.3 Chapter Summary

In this chapter, we successfully extended the max-min robust beamforming approach of [17] into a MIMO-OFDM framework for collaborative transmission systems. We first introduced the system model for an OFDM system over MIMO channels. Based on the system model, we designed a robust beamforming scheme that achieves the best performance under the worst-case CSI mismatch by maximizing the minimum received SNR within a predefined uncertainty region. In addition, the closed-form solution of the max-min optimization problem was presented. It turned out that at each OFDM subcarrier, the robust beamformer distributes the available transmit power across basis beams corresponding to the eigenvectors of the estimated channel correlation matrix in a water-filling fashion. Then, information is sent through the weighted eigenmodes. In addition, we presented analysis of the worst-case error performance for equal power loading and one-directional loading.

Chapter 4

Power Allocation

In Chapter 3, a robust beamforming scheme for collaborative transmission is designed by means of the worst-case performance optimization. At each OFDM subcarrier, the robust beamformer optimally distributes the available transmit power across the eigenmodes according to a water-filling-type process and transmits information through the eigenmodes.

In this chapter, we consider power allocation strategies to distribute the total available power at the transmitter side to subcarriers. We extend the strategies considered in [19,20] for the nonrobust design approach to the case of robust beamforming. Section 4.1 introduces cost functions for power allocation based on the estimated and worst-case OECGs. Section 4.2 presents efficient transmit power allocation strategies based on the maximization of the arithmetic, geometric, and harmonic means and minimum of the cost functions as well as the corresponding closed-form solutions.

4.1 Cost Function

In this section, we formulate two cost functions based on the OECG (3.12) for power allocation. Specifically, the first cost function can be derived by using the presumed channel matrix at the transmitters (3.17) while the second cost function can be obtained by incorporating the worst-case error matrix (3.34).

Assuming that the total power available at the transmitter side is equal to P_0, the global

power constraint can be obtained by summing the average transmit power (3.12) for all k:

$$\sum_{k=1}^{N} \mathrm{tr}\{\mathbf{W}^H(k)\mathbf{W}(k)\} = \sum_{k=1}^{N} p(k) = P_0 \tag{4.1}$$

where $p(k)$ represents the maximum available transmit power at the kth subcarrier as given by (3.49). In other words, the collaborative nodes use the maximum transmit power P_0 to send an OFDM symbol over P time slots.

4.1.1 Estimated Overall Effective Channel Gain

Taking into account the partial knowledge of CSIs at the transmitters $\{\hat{\mathbf{H}}(k)\}_{k=1}^{N}$, the estimated OECG at the kth subcarrier can be expressed as

$$\tilde{\Gamma}(k) = z(k)p(k) \tag{4.2}$$

where

$$z(k) = \mathrm{tr}\left\{\hat{\mathbf{H}}^H(k)\tilde{\mathbf{W}}^H(k)\tilde{\mathbf{W}}(k)\hat{\mathbf{H}}(k)\right\}, \tag{4.3}$$

$$\tilde{\mathbf{W}}(k) = \frac{1}{\sqrt{p(k)}}\mathbf{W}(k), \tag{4.4}$$

and $p(k)$ satisfies the global power constraint (4.1). Note that $\tilde{\mathbf{W}}(k)$ is the normalized beamforming matrix (*i.e.*, $\|\tilde{\mathbf{W}}(k)\|_F = 1$).

4.1.2 Worst-Case Overall Effective Channel Gain

Now considering the worst-case error matrix (3.34) and normalized beamforming matrix (4.4), the worst-case OECG at the kth subcarrier can be rewritten as

$$\tilde{\Gamma}_{\min}(k) = z_{\min}(k)p(k) \tag{4.5}$$

where

$$z_{\min}(k) = \mathrm{tr}\left\{(\hat{\mathbf{H}}(k) + \mathbf{E}_{\min}(k))^H \tilde{\mathbf{W}}^H(k)\tilde{\mathbf{W}}(k)(\hat{\mathbf{H}}(k) + \mathbf{E}_{\min}(k))\right\}, \tag{4.6}$$

and $p(k)$ satisfies the global power constraint (4.1).

4.2 Power Allocation Strategies

In this section, we first consider the maximization of the arithmetic mean of the cost functions, which is the simplest optimization criterion. As can be seen later, the maximization of the geometric mean of the cost functions is equivalent to the classical uniform power allocation among subcarriers. Interestingly, as shown in [20], the maximization of the harmonic mean of the SNR is asymptotically related to the minimization of the mean square error between the estimated signal and the desired signal whereas the maximization of the minimum of the SNR is asymptotically related to the minimization of the SER. Given these motivations, we derive power allocation strategies that maximize the arithmetic, geometric, and harmonic means and minimum of the cost functions, subject to the global power constraint (4.1). In the following, the closed-form solutions to the corresponding design criteria are presented.

4.2.1 Maximization of Arithmetic Mean

First, we consider the arithmetic mean of the estimated OECG of N subcarriers:

$$\frac{1}{N}\sum_{k=1}^{N}\tilde{\Gamma}(k). \tag{4.7}$$

Considering maximization of (4.7), the power allocation problem can be formulated as

$$\begin{aligned} \underset{p(k)}{\text{maximize}} \quad & \sum_{k=1}^{N}\tilde{\Gamma}(k) \\ \text{subject to} \quad & \sum_{k=1}^{N} p(k) = P_0, \\ & p(k) \geq 0, \qquad 1 \leq k \leq N. \end{aligned} \tag{4.8}$$

Since this is a linear programming problem, the optimum solution is to allocate all the available power to the subcarrier which corresponds to the maximum estimated OECG. In this approach, information is transmitted through only one subchannel. The system becomes a single carrier system that wastes the remaining bandwidth. In addition, information on other subcarriers will be lost. Therefore, this approach is not feasible. With the worst-case OECG (4.5), the same result can be obtained.

4.2.2 Maximization of Geometric Mean (GEOM)

In this section, we consider the geometric mean of the cost functions. For the estimated OECG, the geometric mean is given by

$$\left(\prod_{k=1}^{N} \tilde{\Gamma}(k)\right)^{1/N}. \tag{4.9}$$

Taking logarithm of (4.9), it yields

$$\frac{1}{N}\sum_{k=1}^{N} \ln\tilde{\Gamma}(k). \tag{4.10}$$

Since the maximization of (4.9) is equivalent to the maximization of (4.10), we can formulate the optimization problem as

$$\begin{aligned} \underset{p(k)}{\text{maximize}} \quad & \sum_{k=1}^{N} \ln\tilde{\Gamma}(k) \\ \text{subject to} \quad & \sum_{k=1}^{N} p(k) = P_0 \\ & p(k) \geq 0, \qquad 1 \leq k \leq N. \end{aligned} \tag{4.11}$$

Using the Lagrange multiplier method, the corresponding Lagrangian expression can be written as

$$\mathcal{L} = -\sum_{k=1}^{N} \ln\left(z(k)p(k)\right) + \mu\left(\sum_{k=1}^{N} p(k) - P_0\right) \tag{4.12}$$

where μ is the Lagrange multiplier. Differentiating (4.12) with respect to $p(k)$ and equating it to zero, we have that

$$\frac{\partial \mathcal{L}}{\partial p(k)} = -\frac{1}{p(k)} + \mu = 0. \tag{4.13}$$

Then, the optimal solution to this GEOM optimization problem is found to be a uniform power allocation over all subcarriers:

$$p(k) = \frac{P_0}{N} \tag{4.14}$$

which is the simplest power allocation strategy. Note that the same result can be obtained with the worst-case OECG (4.5).

4.2.3 Maximization of Harmonic Mean (HARM)

In this section, we maximize the estimated OECG's harmonic mean, which is given by

$$\left(\frac{1}{N}\sum_{k=1}^{N}\frac{1}{\tilde{\Gamma}(k)}\right)^{-1}. \tag{4.15}$$

The optimization problem can be expressed in the equivalent form as

$$\begin{aligned} \underset{p(k)}{\text{minimize}} \quad & \sum_{k=1}^{N}\tfrac{1}{\tilde{\Gamma}(k)} \\ \text{subject to} \quad & \sum_{k=1}^{N} p(k) = P_0 \\ & p(k) \geq 0, \qquad 1 \leq k \leq N. \end{aligned} \tag{4.16}$$

The solution to this optimization problem can be obtained using the Lagrange multiplier method by minimizing the expression:

$$\mathcal{L} = \sum_{k=1}^{N}\frac{1}{z(k)p(k)} + \mu\left(\sum_{k=1}^{N} p(k) - P_0\right). \tag{4.17}$$

Then, differentiating (4.17) with respect to $p(k)$ yields

$$\frac{\partial \mathcal{L}}{\partial p(k)} = -\frac{1}{z(k)p^2(k)} + \mu. \tag{4.18}$$

Equating (4.18) to zero and solving for $p(k)$, we have

$$p(k) = \frac{1}{\sqrt{\mu z(k)}} \tag{4.19}$$

where

$$\mu = \left(\sum_{k=1}^{N} \frac{P_0^{-1}}{\sqrt{z(k)}} \right)^2 . \tag{4.20}$$

Therefore, the optimal solution to HARM power allocation strategy is given by

$$p(k) = \frac{P_0}{\sum_{i=1}^{N} z^{-\frac{1}{2}}(i)} \frac{1}{\sqrt{z(k)}}. \tag{4.21}$$

Alternatively, the maximization of the harmonic mean of the worst-case OECG (4.5) yields the following closed-form solution:

$$p(k) = \frac{P_0}{\sum_{i=1}^{N} z_{\min}^{-\frac{1}{2}}(i)} \frac{1}{\sqrt{z_{\min}(k)}}. \tag{4.22}$$

These closed-form solutions (4.21) and (4.22) imply that the transmitter allocates more power to subchannels with low gains to maximize the harmonic mean.

4.2.4 Maximization of Minimum (MAXMIN)

The performance of OFDM systems can be substantially degraded by subchannels with low SNRs. In other words, low SNR subchannels are the main contributor to high error rates. Similar to the robust beamforming design approach, we can maximize the minimum of the estimated and worst-case OECGs, subject to the global power constraint (4.1). The optimization problem with the estimated OECG can be formulated in the following form as

$$\begin{aligned} \underset{p(k)}{\text{maximize}} \quad & \min_k \tilde{\Gamma}(k) \\ \text{subject to} \quad & \sum_{k=1}^{N} p(k) = P_0 \\ & p(k) \geq 0, \qquad 1 \leq k \leq N. \end{aligned} \tag{4.23}$$

Introducing a dummy variable t, the original optimization problem (4.23) can be rewritten as [19,29]

$$\begin{aligned} \underset{p(k)}{\text{maximize}} \quad & t \\ \text{subject to} \quad & t \leq z(k)p(k), \quad 1 \leq k \leq N \\ & \sum_{k=1}^{N} p(k) = P_0 \\ & p(k) \geq 0, \quad 1 \leq k \leq N. \end{aligned} \tag{4.24}$$

Since the constraints on t must be satisfied with equality for all k, we have

$$t = z(k)p(k) \quad \forall k. \tag{4.25}$$

Substituting (4.25) into (4.1) and solving for t, we can obtain the constant:

$$t = \frac{P_0}{\sum_{i=1}^{N} z^{-1}(i)}. \tag{4.26}$$

Substituting (4.26) back into (4.25), we obtain the closed-form solution as

$$p(k) = \frac{P_0}{\sum_{i=1}^{N} z^{-1}(i)} \frac{1}{z(k)}. \tag{4.27}$$

Similarly, for the worst-case OECG (4.5), the optimal solution is given by

$$p(k) = \frac{P_0}{\sum_{i=1}^{N} z_{\min}^{-1}(i)} \frac{1}{z_{\min}(k)}. \tag{4.28}$$

As the result of the previous section, it is shown that more transmit power is injected to subchannels with low gains.

4.3 Chapter Summary

In this chapter, we presented power allocation strategies to distribute the total available transmit power to subcarriers. We began by deriving two cost functions to be maximized. Then, we formulated optimization problems using several optimization criteria, including the maximization of the arithmetic, geometric, and harmonic means and the worst-case maximization. In addition, the corresponding closed-form optimal solutions were derived.

Chapter 5

Simulation Results and Discussion

In Chapters 3 and 4, a robust beamforming scheme and several power allocation strategies were presented in the context of collaborative MIMO-OFDM wireless systems. In this chapter, we evaluate the performance of the robust collaborative beamforming system and power allocation strategies through numerical simulations. Section 5.1 introduces a channel model based on the multi-path vector channel simulator [21] and OFDM system parameters. Section 5.2 discusses two approaches to obtain partial CSI. Section 5.3 provides numerical simulation results of the collaborative beamforming system with subcarrier power allocation and detailed discussion of the results.

5.1 Channel Model and Simulation Parameters

The schematic of a system model is given in Fig. 5.1. Note that the details of the collaborative node and the receiver blocks are shown in Fig. 3.2. In the simulations, we consider 4 collaborative nodes ($M_t = 4$) in the x-y plane and a receiver with 2 antennas ($M_r = 2$) located in the far-field along the direction of $\phi = 0°$, where the azimuth angle ϕ is measured from the x-axis. Fig. 5.2 depicts the locations of the collaborative nodes. Note that the locations are chosen from a uniform distribution within a disk of radius $R = 4m$ in the x-y plane. We consider that data are transmitted in frames, which consist of 50 OFDM symbols with $N = 64$ subcarriers. Each OFDM symbol includes 64 signal samples and CP length of 16 samples. Thus, the CP duration is equal to 1/4 of the OFDM symbol duration. We consider an uncoded OFDM system in which each subcarrier transmits independent datastreams. For SER simulations, we use quadrature phase shift keying (QPSK) and

16-QAM signal constellations with a normalized energy, *i.e.*, $E_s = E\{|s(k)|^2\} = 1$. SER simulation results are averaged over more than 3000 Monte-Carlo runs. We consider system bandwidth $B = 20$Mhz, carrier frequency $f_c = 5$GHz, and Doppler frequency $f_d = 10$Hz. A summary of the simulation parameters for OFDM systems and channel is given in Table 5.1.

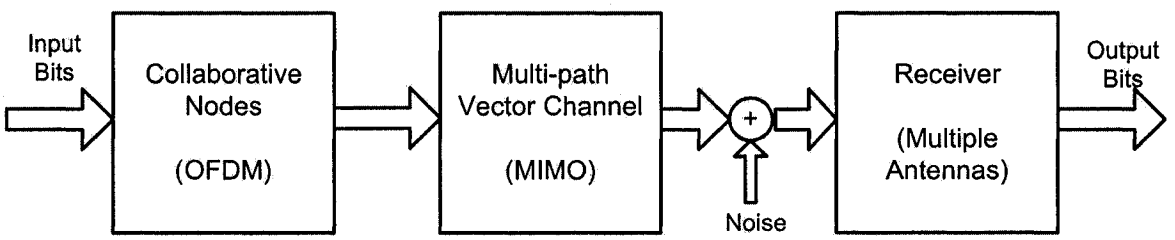

Fig. 5.1 Schematic of a system model.

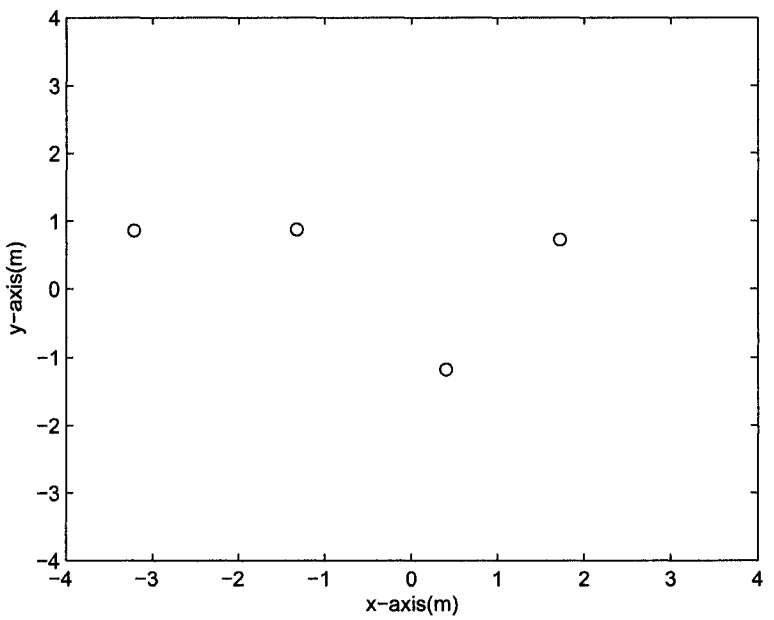

Fig. 5.2 Location of collaborative nodes.

Table 5.1 Simulation Parameters

Parameters	Values
System Bandwidth	20MHz
Carrier Frequency	5GHz
Sampling Time	50ns
OFDM Subcarriers	64
CP length	16
OFDM Symbol Duration	$4\mu s$
Useful Data Period	$3.2\mu s$
CP Period	$0.8\mu s$
Doppler Spread	10Hz
Coherence Time	42.3ms
Symbol Constellation	QPSK/16-QAM
Channel Coding	Uncoded

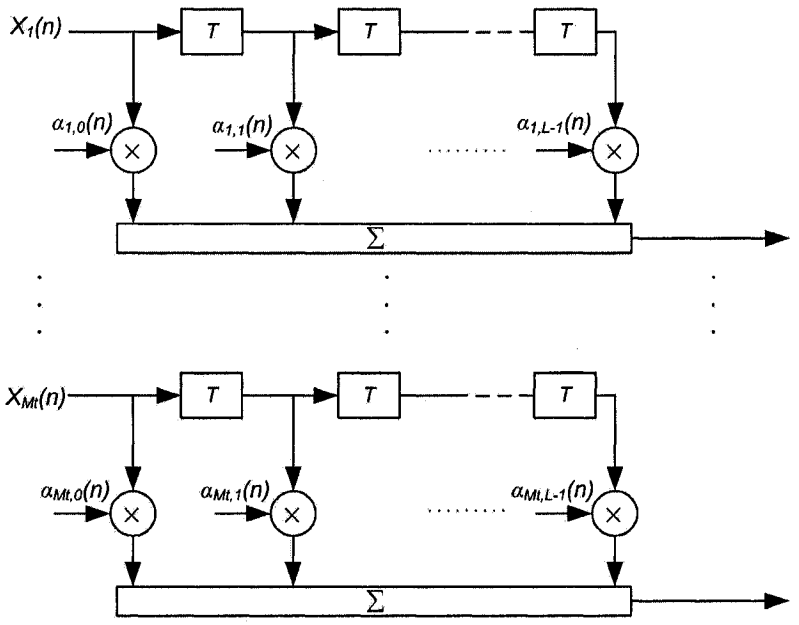

Fig. 5.3 Multi-path vector channel.

Transmission channels between the collaborative nodes and the receiver are generated using a statistical multi-path vector channel simulator [21]. Fig. 5.3 shows the block diagram of a multi-path vector channel model. We assume that channels are fixed in a frame, but can vary between successive frames. In addition, all available channels are assumed to have the same exponential power delay profile with $L = 3$ resolvable taps. The corresponding mean angle of arrival is set to 0°, 25°, 50° with angular spread 5°, 10°, 20°, respectively. The tapped delay line model for the jth channel can be expressed as

$$g_j(n,\tau) = \sum_{l=0}^{L-1} \alpha_{j,l}(n)\delta(\tau - lT) \tag{5.1}$$

where $\alpha_{j,l}(n)$ is the time-varying complex gain of path l for the jth channel. Let $\mathbf{g}_j^{(m)} = [g_j^{(m)}(0), g_j^{(m)}(1), \ldots, g_j^{(m)}(L-1)]^T$ be the baseband sampled channel impulse response between the mth node and the jth receive antenna. The frequency response of the channel

at the kth subcarrier can be expressed as

$$h_j^{(m)}(k) = \sum_{n=0}^{L-1} g_j^{(m)}(n) e^{-\frac{j2\pi kn}{N}} = \mathbf{f}^H(k)\mathbf{g}_j^{(m)} \tag{5.2}$$

where $\mathbf{f}(k) = [1, e^{\frac{j2\pi k}{N}}, \ldots, e^{\frac{j2\pi kL}{N}}]^T$. Hence, we can obtain the $M_t \times M_r$ channel matrices $\{\mathbf{H}(k)\}_{k=1}^N$ whose entries are given by (5.2).

We suppose that the transmitters have only access to the estimated CSI $\{\hat{\mathbf{H}}(k)\}_{k=1}^N$ but the receiver has perfect knowledge of $\{\mathbf{W}(k), \mathbf{H}(k)\}_{k=1}^N$ for MRC. Without loss of generality, the estimated CSI matrices are normalized to 1 such that $0 \leq \{\varepsilon(k)\}_{k=1}^N \leq 1$. As in [17], we consider the sizes of the uncertainty region $\{\varepsilon(k)\}_{k=1}^N$ as robust design parameters. At low SNRs, the performance of the system is mainly dominated by the noise. It is sufficient to use small values of $\varepsilon(k)$ such that the nonrobust beamforming is applied. In contrast, at high SNRs, the mismatch between the presumed and true CSI is the dominant factor that degrades the system performance. Hence, larger values of $\varepsilon(k)$ should be used.

5.2 Partial CSI

In the following, we discuss two approaches to obtain the partial CSI, as needed for the evaluation of the collaborative system.

5.2.1 Downlink Measurements

We consider the case where the receiver periodically sends pilot signals to the transmitters. Then, the received pilot signals can be exploited to estimate the downlink channels at the transmitters. Since there will be a correlation between the downlink and uplink channels, the uplink channels can also be estimated through minimum mean square error (MMSE) estimation [14,32]. Hence, the true channel $\mathbf{H}(k)$ can be expressed in terms of the channel estimate $\hat{\mathbf{H}}(k)$ and the estimation error $\mathbf{E}(k)$:

$$\mathbf{H}(k) = \hat{\mathbf{H}}(k) + \mathbf{E}(k), \quad 1 \leq k \leq N \tag{5.3}$$

where $\mathbf{E}(k)$ is a random matrix whose entries are i.i.d. ZMCSCG random variables with variance σ_e^2.

5.2.2 Delayed Channel Feedback

In the delayed channel feedback scenario, the receiver is assumed to have perfect estimates of the channel and send them back to the transmitters through an error-free feedback channel with some time delay. This time delay can be modeled by a loss of correlation of the error-free feedback. Thus, the delayed feedback channel can be modeled using the first order autoregressive model [14, 15, 33]:

$$\hat{\mathbf{H}}(k) = \rho \mathbf{H}(k) + \sqrt{1-\rho^2}\mathbf{X}(k) \tag{5.4}$$

where $\mathbf{X}(k)$ is a random matrix with each entry drawn from an i.i.d. ZMCSCG random process with unit variance and ρ is the correlation coefficient between the channel feedback and true channel ($0 \leq \rho \leq 1$). The correlation coefficient specified by the Jakes' model is given by [27]

$$\rho = J_0(2\pi f_d \tau_d) \tag{5.5}$$

where f_d and τ_d are the Doppler frequency and feedback delay, respectively. In particular, when ρ is 0, the transmitters have no CSI information. With $\rho = 1$, this implies that full channel knowledge is available at the transmitters. Hence, the correlation coefficient is a measure of the feedback quality.

5.3 Results and Discussion

5.3.1 Robust Beamforming

We compare the performance of a robust beamforming approach with two nonrobust beamforming approaches: conventional one-directional beamforming and equal-power beamforming (transmit power is evenly distributed among all eigenmodes). We first consider a uniform transmit power allocation (GEOM) over all subcarriers (see Section 4.2.2).

Figs. 5.4, 5.5, and 5.6 show the uncoded average SER performance using QPSK and 16-QAM constellations for Gaussian channel uncertainty with variance $\sigma_e^2 = 0.4$ and delayed feedback channel with correlation coefficients $\rho = 0.85$ and 0.75, respectively. In the simulations, we linearly increase $\{\varepsilon(k)\}_{k=1}^{N}$ from 0 to 0.95 over the E_s/N_0 range of 10 to 17dB for 16 QAM and over the E_s/N_0 range of 5 to 11dB for QPSK. We observe that the cases for Gaussian channel uncertainty with variance $\sigma_e^2 = 0.4$ and delayed feedback channel with

correlation coefficient $\rho = 0.85$ provide very similar performance results. Importantly, the figures show that the robust beamformer offers performance gains over the one-directional and equal-power beamformers. This is due to the fact that the robust beamformer effectively distributes the transmit power among available estimated eigenmodes of the channel whereas the conventional one-directional beamformer uses only the maximum estimated eigenmode and the equal-power beamformer does not utilize the CSI. The performance of the equal-power beamformer approaches that of the robust beamformer at high SNRs. Fig. 5.7 shows the SER performance for a Rician fading channel with the Rician factor $\mathcal{K} = [1\ 0\ 0]$ (a line-of-sight component is only added to the first channel tap coefficient) and correlation coefficient $\rho = 0.85$. We also find similar performance results.

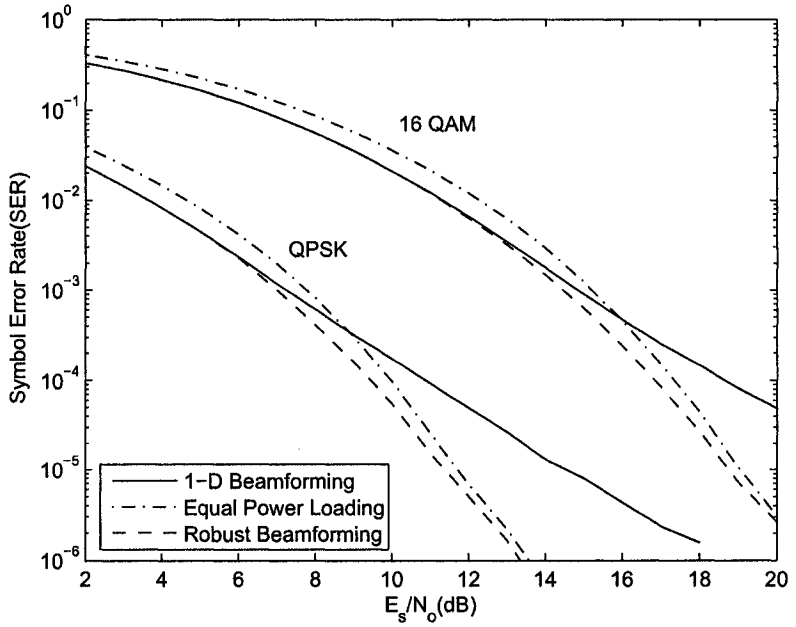

Fig. 5.4 SER vs. E_s/N_0 for Gaussian channel uncertainty with $\sigma_e^2 = 0.4$.

Fig. 5.8 depicts the pdf of the SNR at the MRC output of the receiver when $E_s/N_0 =$ 16dB, $k = 40$, $\rho = 0.85$, and $\varepsilon(k) = 0.95$. Note that the pdf is calculated from 50000 Monte-Carlo runs, the vertical lines represent the corresponding SNR means, and the embedded plot in Fig. 5.8 shows the pdf in the SNR range between 12 dB and 16 dB. This figure verifies that the conventional one-directional beamformer is optimal in terms of the expected SNR. However, the SER performance of the one-directional beamformer is poor as seen in

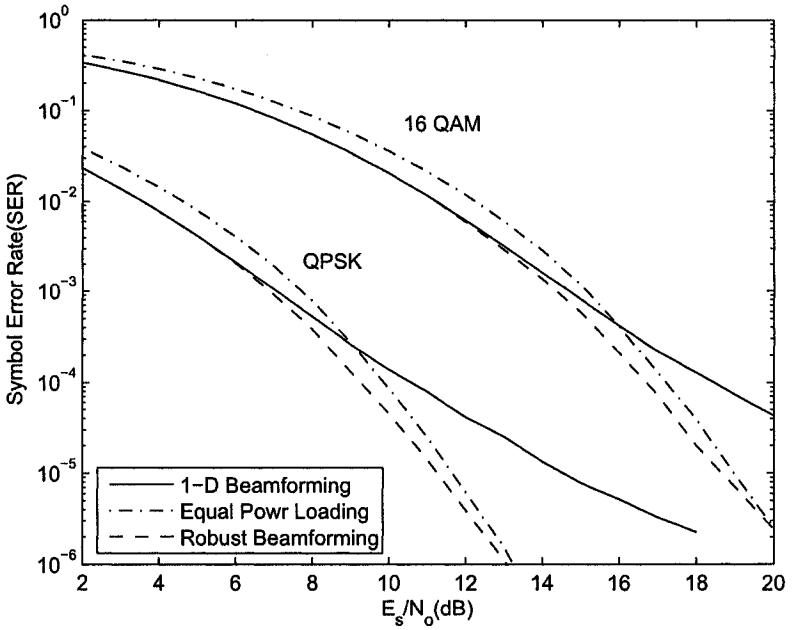

Fig. 5.5 SER vs. E_s/N_0 for delayed channel feedback with $\rho = 0.85$.

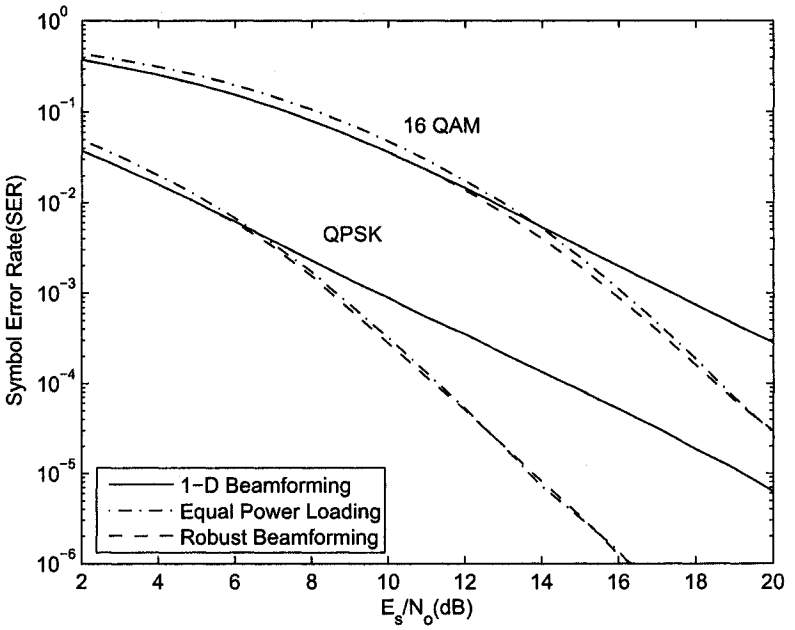

Fig. 5.6 SER vs. E_s/N_0 for delayed channel feedback with $\rho = 0.75$.

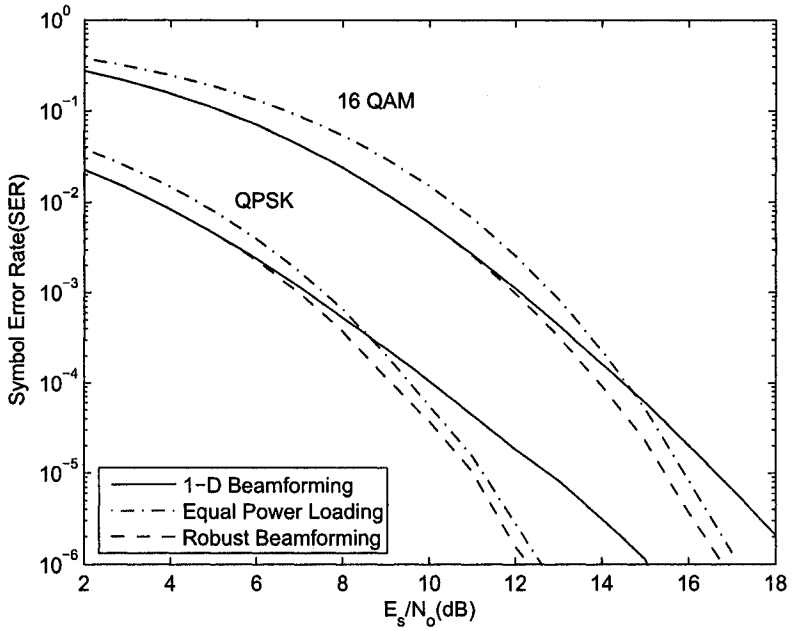

Fig. 5.7 SER vs. E_s/N_0 for the Rician factor $\mathcal{K} = [1\ 0\ 0]$ and $\rho = 0.85$.

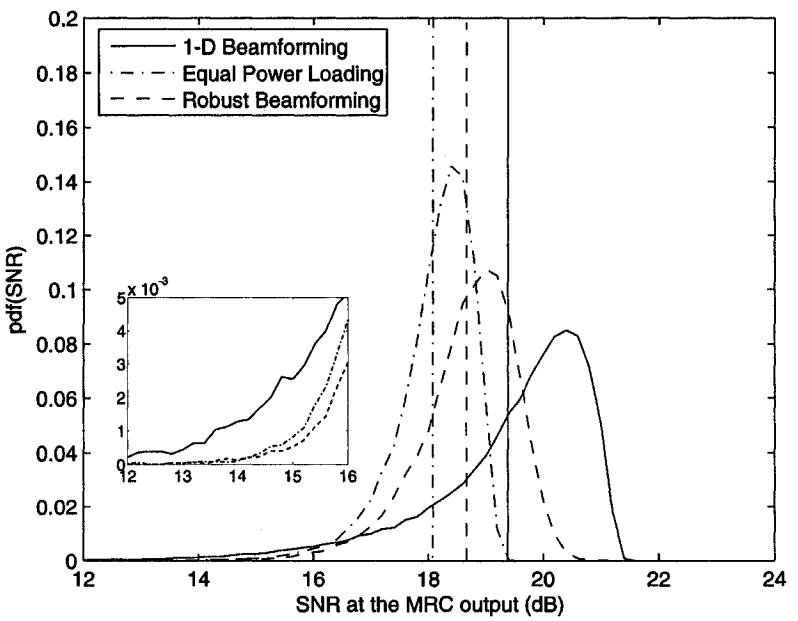

Fig. 5.8 SNR pdf at the MRC output ($E_s/N_0 = 16$dB, $k = 40$, $\rho = 0.85$).

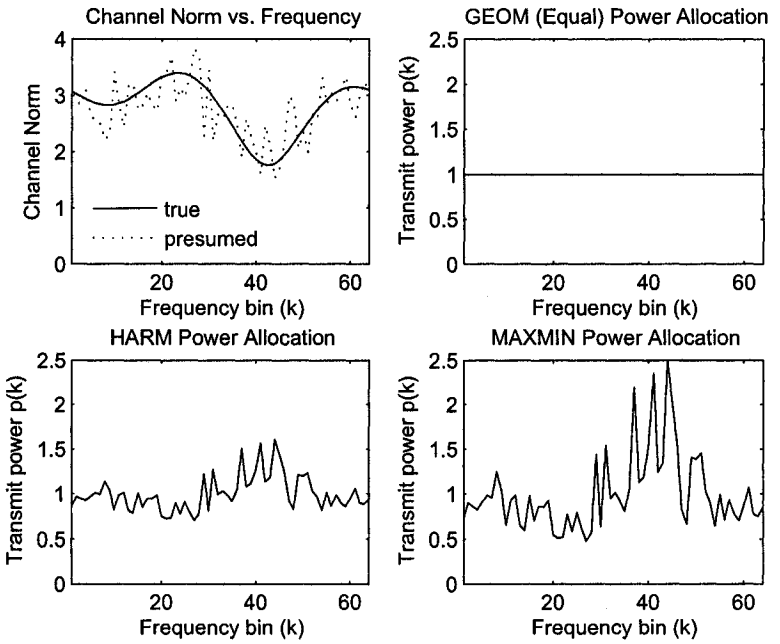

Fig. 5.9 Power allocation strategies ($P_0 = 64$W).

the previous simulations. This is because the SER performance is dominated by worst-case errors (performance). Thus, maximizing the expected SNR may not guarantee the lowest SER performance. The SNR variance must be kept as small as possible to improve the SER. One possible solution is to find a tradeoff between high SNR mean and low SNR variance. Indeed, the robust beamformer provides a tradeoff between the mean and variance by maximizing worst-case performance as seen in Fig. 5.8.

5.3.2 Power Allocation

In this section, we compare the performance of the power allocation strategies (GEOM, HARM, and MAXMIN) based on the SER obtained by incorporating these strategies into the robust beamformer. We consider only the delayed feedback channel scenario and the location of the nodes depicted in Fig. 5.2. A 16-QAM constellation is used for the SER simulations.

Fig. 5.9 shows the allocated power to the N subcarriers using the estimated OECG (see Section 4.1.1) when the total transmit power is $P_0 = 64$W and $\rho = 0.85$. The top left figure

shows the Frobenius norm of the true channel $\|\mathbf{H}(k)\|_F$ and the presumed channel $\|\hat{\mathbf{H}}(k)\|_F$ for a given channel realization. With the GEOM technique, the total transmit power is evenly distributed to all subcarriers. With the HARM and MAXMIN techniques, however, more power is injected to the subcarriers in deep fades as expected from the expressions (4.21) and (4.27).

Figs. 5.10 and 5.11 depict the uncoded average SER performance with subcarrier power allocation with correlation coefficients $\rho = 0.85$ and 0.75, respectively. Abbreviations used in the figures are explained as follows: one-directional beamforming and uniform power allocation among subcarriers (1-D + GEOM), equal-power beamforming and uniform power allocation among subcarriers (Equal Power Loading + GEOM), robust beamforming and uniform power allocation among subcarriers (Robust + GEOM), robust beamforming and HARM power allocation among subcarriers using the estimated OECG (Robust + HARM(estimated OECG)), robust beamforming and MAXMIN power allocation among subcarriers using the estimated OECG (Robust + MAXMIN(estimated OECG)), robust beamforming and HARM power allocation among subcarriers using the perfect OECG (Robust + HARM(perfect OECG)), and robust beamforming and MAXMIN power allocation among subcarriers using the perfect OECG (Robust + MAXMIN(perfect OECG)). It is evident that combining the HARM and MAXMIN power allocation strategies with robust beamforming can substantially increase the system performance by injecting more power to subchannels experiencing deep fades. The MAXMIN technique performs better than the HARM technique. However, it should be noted that power allocation strategies based on the exact CSI (perfect OECG) can further improve the system performance by approximately 2dB at high SNRs.

So far the power allocation strategies which maximize the estimated OECG have been investigated through numerical simulations. The HARM and MAXMIN techniques have been shown to increase the performance of the collaborative beamforming system. Now we investigate the performance of the robust beamformer using the worst-case OECG (see Section 4.1.2) for subcarrier power allocation. Figs. 5.12 and 5.13 plot the uncoded average SER performance for correlation coefficients $\rho = 0.85$ and 0.75, respectively. It can be seen that power allocation approaches based on the worst-case OECG slightly outperform those based on the estimated OECG, but the performance difference between them is very small.

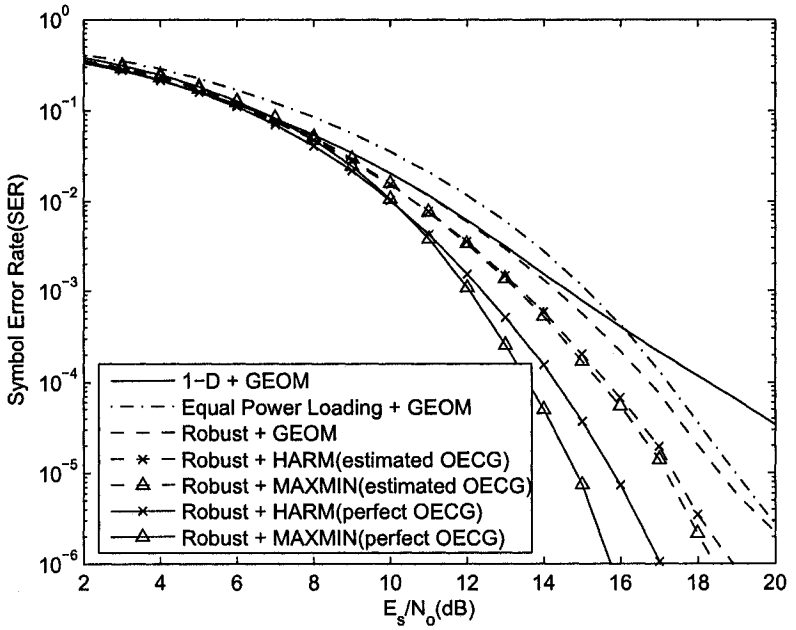

Fig. 5.10 SER vs. E_s/N_0 for subcarrier power allocation ($\rho = 0.85$).

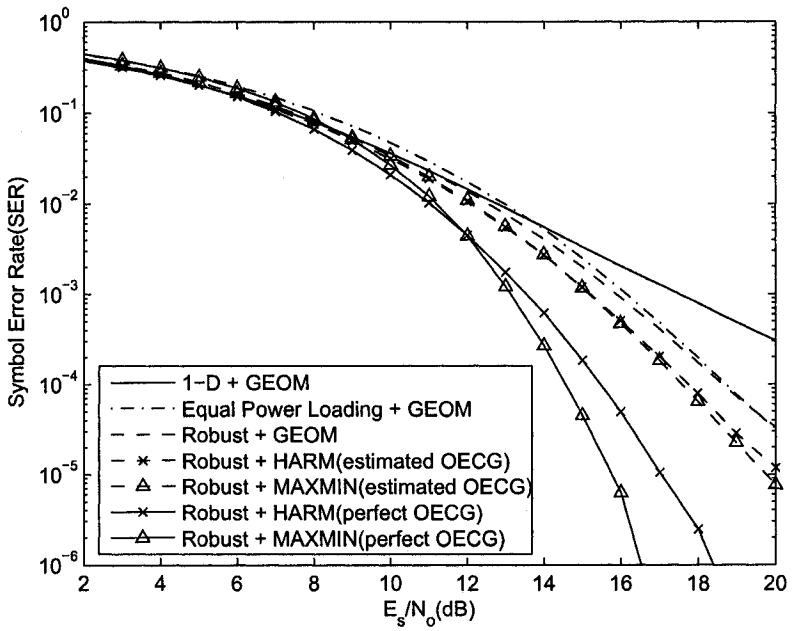

Fig. 5.11 SER vs. E_s/N_0 for subcarrier power allocation ($\rho = 0.75$).

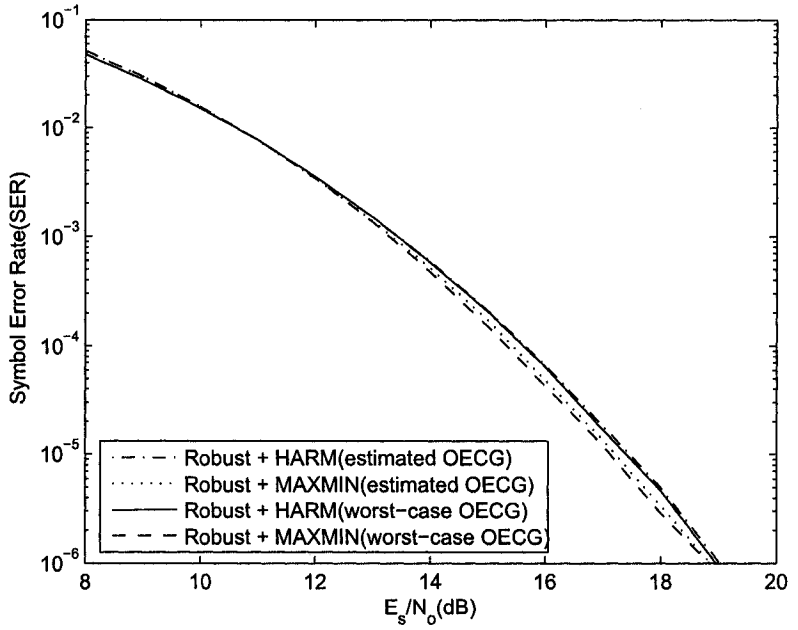

Fig. 5.12 SER for the estimated and worst-case OECGs ($\rho = 0.85$).

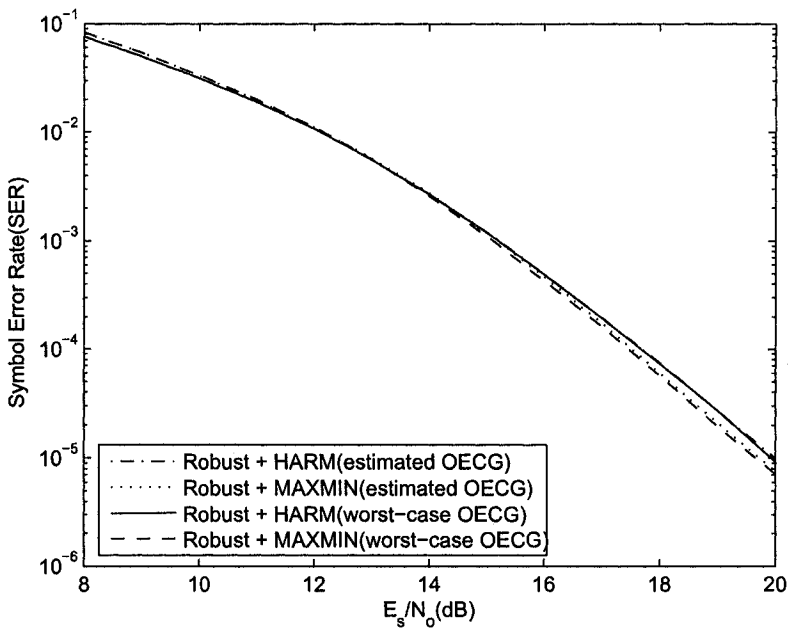

Fig. 5.13 SER for the estimated and worst-case OECGs ($\rho = 0.75$).

5.4 Chapter Summary

In this chapter, we investigated the performance of robust beamforming for collaborative MIMO-OFDM wireless systems. Through numerical simulations, we evaluated its robust performance against CSI errors. The robust beamformer outperformed the conventional one-directional and equal-power beamformers. In addition, we showed that combining the HARM and MAXMIN power allocation strategies with the robust beamformer can significantly increase the system performance by injecting more power to subchannels experiencing deep fades. The MAXMIN strategy performed better than the HARM strategy. Moreover, our numerical simulations showed that power allocation approaches based on the worst-case OECG slightly outperform those based on the estimated OECG.

Chapter 6

Conclusion

This thesis has focused on the design and evaluation of a beamforming scheme that is robust against CSI mismatches and applicable to practical collaborative wireless systems. The main aim for this thesis was to extend the max-min robust beamforming design approach of [17] into a MIMO-OFDM framework for collaborative transmission systems and to apply the power allocation strategies considered in [19, 20] for the nonrobust design approach to the case of robust beamforming.

This chapter presents a brief summary of the thesis work and gives future research directions.

6.1 Thesis Summary

This thesis began by first reviewing the properties of collaborative beamforming and basic principles of OFDM. It was shown that collaborative beamforming using randomly distributed nodes can achieve an average beampattern with a narrow mainlobe, low sidelobes, and a high directivity by forming a virtual antenna array. In addition, collaborative beamforming was shown to be robust to synchronization errors among collaborating nodes and provide a significant beamforming gain. Then, orthogonality of carriers, implementation of baseband OFDM transceivers, including generation and demodulation of an OFDM signal, and benefits of CP were discussed.

In Chapter 3, a robust beamforming scheme for collaborative MIMO-OFDM wireless systems was designed by means of the max-min robust design approach of [17]. Specifically, at each OFDM subcarrier, the robust beamformer was designed to maximize the

minimum received SNR within a predefined uncertainty region, whose size is considered as a robust design parameter. The optimal power loading solution obtained using the KKT optimality conditions was viewed as a form of water-filling. Thus, the robust beamformer was designed to distribute the available transmit power across basis beams corresponding to the eigenvectors of the channel correlation matrix perceived by the transmitters in a water-filling fashion according to the water-level and transmit data along the basis beams (eigenmodes). In addition, it was shown that the robust beamformer utilizes full eigenmodes of the MIMO channel while the classical nonrobust beamformer uses only the dominant eignemode. Analysis of the worst-case error performance for equal power loading and one-directional loading was presented.

To improve the performance of the collaborative beamforming system, several subcarrier power allocation strategies were investigated based on optimization criteria used in [19,20] for nonrobust beamforming, including the maximization of the arithmetic, geometric, and harmonic means and the worst-case maximization. Using the estimated and worst-case OECGs, the closed-form optimal solutions were derived. The GEOM technique was found to be a uniform power allocation over all subcarriers. The HARM and MAXMIN techniques were shown to inject more transmit power to the subcarriers where deep fading occurs.

To evaluate the performance of the robust beamformer and power allocation strategies, SER performance results obtained from Monte-Carlo simulations were used. The robust OFDM beamformer was tested under downlink measurements and delayed channel feedback scenarios. A statistical multi-path vector channel simulator was used to model MIMO frequency-selective fading channels. Through numerical simulations, it was shown that the robust beamformer offers performance gains over the conventional one-directional and equal-power beamformers and provides a tradeoff between the SNR mean and SNR variance by the worst-case optimization. In addition, it was shown that the use of the HARM and MAXMIN power allocation strategies improves the performance of the collaborative beamforming system by injecting more power to subcarriers corresponding to deep fades as expected. The MAXMIN strategy has performed better than the HARM strategy. Moreover, the HARM and MAXMIN power allocation approaches based on the worst-case OECG were shown to slightly outperform those based on the estimated OECG.

6.2 Future Research Directions

This thesis has looked at narrowband fixed transmit beamforming and subcarrier power allocation schemes in a collaborative MIMO-OFDM wireless system. There are still enormous potential benefits to be obtained from collaborative beamforming in cooperative communications.

Some possible future research works include:

- Incorporation of STBC into collaborative beamforming in order to compensate for the data rate loss incurred during spreading.
- Performance analysis of synchronization errors on collaborative beamforming for MIMO-OFDM systems. Synchronization errors may include carrier phase and frequency offset, and symbol time error.
- Design of blind collaborative beamforming for MIMO-OFDM systems that doest not rely on *a priori* knowledge of node locations and channel responses. Blind beamforming for distributed sensor networks is discussed in [34].
- Design of adaptive collaborative beamforming for MIMO-OFDM systems that keeps track of changes in signal characteristics and collaborative communications environment.

References

[1] J. C. Chen, K. Yao, and R. E. Hudson, "Source localization and beamforming," *IEEE Signal Processing Mag.*, vol. 19, pp. 30–39, Mar. 2002.

[2] C. Chong and S. P. Kumar, "Sensor networks: evolution, opportunities and challenges," *Proceedings of the IEEE*, vol. 91, pp. 1247–1256, Aug. 2003.

[3] A. Nosratinia, T. E. Hunter, and A. Hedayat, "Cooperative communication in wireless networks," *IEEE Commun. Mag.*, vol. 42, pp. 74–80, Oct. 2004.

[4] H. Ochiai, P. Mitran, H. V. Poor, and V. Tarokh, "Collaborative beamforming in ad hoc networks," *in Proc. IEEE Inform. Theory Workshop (ITW'04)*, pp. 396–401, Oct. 2004.

[5] H. Ochiai, P. Mitran, H. V. Poor, and V. Tarokh, "On the effects of phase estimation errors on collaborative beamforming in wireless ad hoc networks," *in Proc. IEEE Int. Conf. on Acoust., Speech, Signal Processing (ICASSP '05)*, pp. iii/657–iii/660, Mar. 2005.

[6] H. Ochiai, P. Mitran, H. V. Poor, and V. Tarokh, "Collaborative beamforming for distributed wireless ad hoc sensor networks," *IEEE Trans. Signal Processing*, vol. 53, pp. 4110–4124, Nov. 2005.

[7] G. Barriac, R. Mudumbai, and U. Madhow, "Distributed beamforming for information transfer in sensor networks," *in Proc. 3rd Int. Symp. on Information Processing in Sensor Networks (IPSN'04)*, pp. 81–88, Apr. 2004.

[8] B. Ananthasubramaniam, G. Barriac, R. Mudumbai, and U. Madhow, "Distributed space-time communication for sensor networks," *in Proc. 1st Int. Symmp. on Control, Communications and Signal Processing (ISCCSP'04)*, pp. 195–198, Mar. 2004.

[9] R. Mudumbai, G. Barriac, and U. Madhow, "On the feasibility of distributed beamforming in wireless networks," *IEEE Trans. Wireless Commun.*, vol. 6, pp. 1–10, Apr. 2007.

[10] R. Mudumbai, J. Hespanha, U. Madhow, and G. Barriac, "Scalable feedback control for distributed beamforming in sensor networks," *in Proc. Int. Symp. on Information Theory (ISIT'05)*, pp. 137–141, Sep. 2005.

[11] R. Mudumbai, J. Hespanha, U. Madhow, and G. Barriac, "Distributed transmit beamforming using feedback control," *IEEE Trans. Inform. Theory.* (submitted for review).

[12] R. Mudumbai, B. Wild, U. Madhow, and K. Ramchandran, "Distributed beamforming using 1 bit feedback: from concept to realization," *in Proc. 44th Allerton Conf. on Communication Control and Computing*, Sep. 2006.

[13] S. Luskey, C. Jin, and A. Schaik, "Energy savings from implementing collaborative beamforming for a remote low power wireless sensor network," *in Proc. 1st IEEE Int. Conf. on Wireless Broadband and Ultra Wideband Communications (AusWireless'06)*, Mar. 2006.

[14] S. Zhou and G. B. Giannakis, "Optimal transmitter eigen-beamforming and space-time block coding based on channel mean feedback," *IEEE Trans. Signal Processing*, vol. 50, pp. 2599–2613, Oct. 2002.

[15] P. Xia, S. Zhou, and G. B. Giannakis, "Adaptive MIMO-OFDM based on partial channel state information," *IEEE Trans. Signal Processing*, vol. 52, pp. 202–213, Jan. 2004.

[16] S. Shahbazpanahi, A. B. Gershman, Z. Luo, and K. M. Wong, "Robust adaptive beamforming for general-rank signal models," *IEEE Trans. Signal Processing*, vol. 51, pp. 2257–2269, Sep. 2003.

[17] A. Abdel-Samad, T. N. Davidson, and A. B. Gershman, "Robust transmit eigen beamforming based on imperfect channel state information," *IEEE Trans. Signal Processing*, vol. 54, pp. 1596–1609, May 2006.

[18] A. Abdel-Samad and A. B. Gershman, "Robust transmit eigen-beamforming with imperfect knowledge of channel correlations," *in Proc. IEEE Intl. Conf. on Commun. (ICC'05)*, vol. 4, pp. 2292–2296, May 2005.

[19] D. P. Palomar, J. M. Cioffi, and M. A. Lagunas, "Joint Tx-Rx beamforming design for multicarrier MIMO channels: A unified framework for convex optimization," *IEEE Trans. Signal Processing*, vol. 51, pp. 2381–2401, Sep. 2003.

[20] A. Pascual-Iserte, A. I. Perez-Neira, and M. A. Lagunas, "On power allocation strategies for maximum signal to noise and interference ratio in an OFDM-MIMO system," *IEEE Trans. Wireless Commun.*, vol. 3, pp. 808–820, May 2004.

[21] A. Stephenne and B. Champagne, "Effective multi-path vector channel simulator for antenna array systems," *IEEE Trans. Veh. Technol.*, vol. 49, pp. 2370–2381, Nov. 2000.

[22] H. L. Van Trees, *Optimum Array Processing.* John Wiley & Sons, 2002.

[23] A. Papoulis and U. Pillai, *Probability, Random Variables and Stochastic Processes.* McGraw-Hill, 2002.

[24] A. Goldsmith, *Wireless Communications.* Cambridge University Press, 2005.

[25] A. Molisch, *Wireless Communications.* Wiley-IEEE Press, 2005.

[26] A. Paulraj, R. Nabar, and D. Gore, *Introduction to Space-Time Wireless Communications.* Cambridge University Press, 2003.

[27] J. G. Proakis, *Digital Communications.* McGraw-Hill, 2001.

[28] S. Zhou and G. B. Giannakis, "Optimal transmitter eigen-beamforming and space-time block coding based on channel correlations," *IEEE Trans. Inform. Theory*, vol. 49, pp. 1673–1690, July 2003.

[29] A. Pascual-Iserte, D. P. Palomar, A. I. Perez-Neira, and M. A. Lagunas, "A robust maximin approach for MIMO communications with imperfect channel state information based on convex optimization," *IEEE Trans. Signal Processing*, vol. 54, pp. 346–360, Jan. 2006.

[30] A. Hjorungnes and D. Gesbert, "Complex-valued matrix differentiation: Techniques and key results," *IEEE Trans. Signal Processing*, vol. 55, pp. 2740–2746, Jun. 2007.

[31] S. Boyd and L. Vandenberghe, *Convex Optimization.* Cambridge University Press, 2004.

[32] J. K. Cavers, "Single-user and multiuser adaptive maximal ratio transmission for rayleigh channels," *IEEE Trans. Veh. Technol.*, vol. 49, pp. 2043–2050, Nov. 2000.

[33] J. Choi and R. W. Heath, "Interpolation based transmit beamforming for MIMO-OFDM with limited feedback," *IEEE Trans. Signal Processing*, vol. 54, pp. 4125–4135, Nov. 2005.

[34] K. Yao, R. E. Hudson, C. W. Reed, D. Chen, and F. Lorenzelli, "Blind beamforming on a randomly distributed sensor array system," *IEEE J. Select. Areas Commun.*, vol. 16, pp. 1555–1567, Oct. 1998.